

2017

From Gd₂O₃suspension to nanocomposite: Synthesis, properties and radiation protection

Ly B. T. La
Edith Cowan University

Follow this and additional works at: <https://ro.ecu.edu.au/theses>



Part of the [Engineering Commons](#), and the [Radiology Commons](#)

Only chapters 1, 3 and 8 are available in this version of the thesis.

Chapters 4, 5, and 7 have been published and are listed under "Related publications", with links provided to both the published and the Green open access versions.

Recommended Citation

La, L. B. (2017). *From Gd₂O₃suspension to nanocomposite: Synthesis, properties and radiation protection*. <https://ro.ecu.edu.au/theses/2019>

This Thesis is posted at Research Online.
<https://ro.ecu.edu.au/theses/2019>

Edith Cowan University

Copyright Warning

You may print or download ONE copy of this document for the purpose of your own research or study.

The University does not authorize you to copy, communicate or otherwise make available electronically to any other person any copyright material contained on this site.

You are reminded of the following:

- Copyright owners are entitled to take legal action against persons who infringe their copyright.
- A reproduction of material that is protected by copyright may be a copyright infringement. Where the reproduction of such material is done without attribution of authorship, with false attribution of authorship or the authorship is treated in a derogatory manner, this may be a breach of the author's moral rights contained in Part IX of the Copyright Act 1968 (Cth).
- Courts have the power to impose a wide range of civil and criminal sanctions for infringement of copyright, infringement of moral rights and other offences under the Copyright Act 1968 (Cth). Higher penalties may apply, and higher damages may be awarded, for offences and infringements involving the conversion of material into digital or electronic form.

**From Gd_2O_3 suspension to nanocomposite:
synthesis, properties and radiation protection**

This thesis is presented in fulfilment of the requirements

for the degree of

Doctor of Philosophy

By

Ly Bao Truc La

Edith Cowan University

School of Engineering

2017

DISCLAIMER

I hereby declare that any ideas, analysis and discussion in this thesis are my own work, otherwise clearly referenced, and abide by University's Plagiarism policy.

Signed:



La, Bao Truc Ly

October 04th, 2017

USE OF THESIS

The Use of Thesis statement is not included in this version of the thesis.

ABSTRACT

This study provides details for the design, preparation of an environmentally friendly, clinically safe and lightweight radiation protective shield made of Gd_2O_3 /epoxy nanocomposite (Gd-nanocomposite) which is proposed as an alternative to traditional toxic lead (Pb)-based aprons for diagnostic X-ray protection. In theory, this particulate nanocomposite can possess significant features of both inorganic particles and organic polymeric matrices. However, in practice, its performance does not simply depend on the sum of the individual contributions of characteristics of the constituent phases but on the interaction of their inner interfaces and the homogeneous dispersion of inorganic particles in the polymer matrix.

The miniaturization of inorganic particles to nanoscale before mixing with an organic matrix has been considered as an effective way to improve the interface of the dispersion phase. Unfortunately, homogeneous dispersion has still not yet been achieved in this type of material due to the coalescence of nanoparticles resulting from the large surface area of nanoparticles and their chemical incompatibility with the matrix. The effect of inter-particle forces arising from adsorbed typical cationic and anionic surfactants on the morphology of the ball milled gadolinium oxide (Gd_2O_3) is investigated to attain the optimal conditions for interface improvement between Gd_2O_3 particles and an epoxy matrix.

The experimental outcomes are interpreted in terms of the stabilization and interaction mechanisms of the fine washed Gd_2O_3 particles (size diameter $<1\mu m$) in an aqueous medium under the variation of the surface forces arising from adsorbed surfactants. The point of zero charge or isoelectric point (IEP) of ball milled Gd_2O_3 particles suspension is at pH 11. In the presence of adsorbed anionic SDS (Sodium dodecyl sulphate), the particles are refined together with numerous 2D nanowire or nano-rod particles at pH ~ 8 . In contrast, the coarser particles are found when cationic CTAB (Cetyl trimethylammonium bromide) is used to modify the Gd_2O_3 surface. This is invoked from organic shell formed by the high adsorbability of negatively charged heads of SDS into the bare positive charge density of the particle. This capping agent acts as (i) a steric barrier preventing the agglomeration or re-welding of the powder during nanoparticle preparation and (ii) an intermediate adhesive that enhances the miscibility of the particle and liquid matrix, thereby improving the particle dispersion in the organic matrix.

Based on the above outcomes, an optimal geometric design of a non-lead based X-ray protective material with lightweight per volume unit is prepared. A plateau with 28-30% increments in the value of fracture toughness (K_{IC} (Mpa.m^{1/2})) is observed with a specific addition of 0.08 to 0.1 volume fraction (ϕ_s) of SDS-encapsulated Gd₂O₃ particles in pure epoxy. The same quantity of particles also optimally raises the critical strain energy release rate (G_{IC} (J.m⁻²)) and Young's modulus (E (MPa)) of epoxy by approximately 22-24% and 18-25% respectively. A 16 mm thick sheet of fabricated filled composite at ϕ_s of 0.08 and 0.1 can shield greater than 95% (0.5 mm Pb-equivalence) and 99% (1 mm Pb-equivalence) respectively of a primary X-ray beam in the range of 60-120kVp. At the same X-ray attenuation (99% attenuation), the specimen is 7, 8.5, and 16 times lighter than wood, glass, and concrete respectively. At 0.5 mm Pb-equivalence, the composite also has 4.5-19.4% less weight per unit area than current commercial non-lead products.

ACKNOWLEDGEMENT

I appreciate Edith Cowan University, Australia and Vietnamese government for financially supporting this research through an ECU-VIED joint postgraduate scholarship. I also thank for laboratory support for X-ray test from Department of Medical Engineering and Physics, Royal Perth Hospital. I especially acknowledge the enthusiastic support and supervision of Professor Laichang Zhang, Dr Kevin Hayward (Edith Cowan University) and Professor Yee-Kwong Leong (University of Western Australia) during my PhD journey. Their valuable advice assists to carry out a quality research. I am grateful to coordinative technical support from Mr. Adrian Styles, Dr. Hellen Renwick, and my lab mates at Edith Cowan University and the University of Western Australia. I am grateful to all my friends and colleagues in Can Tho University of Technology, Vietnam for their mental support throughout this research journey. Last but not least, I express my sincere gratitude to my husband for his love and commitment throughout my research.

PUBLICATIONS BASED ON THE PRESENT WORK

- [1] L. B. T. La, Y. K. Leong, C. Leatherday, P. I. Au, K. J. Hayward, and L. C. Zhang, "X-ray protection, surface chemistry and rheology of ball-milled submicron Gd_2O_3 aqueous suspension," *Colloids and Surfaces A: Physicochemical and Engineering Aspects*, vol. 501, pp. 75-82, 2016.
- [2] L. B. T. La, Y. K. Leong, H. P. Watts, P. I. Au, K. J. Hayward, and L. C. Zhang, "A novel approach for the preparation of nanosized Gd_2O_3 structure: the influence of surface force on the morphology of ball milled particles," *Colloids and Surfaces A: Physicochemical and Engineering Aspects*, vol. 506, pp. 13-19, 2016.
- [3] L. B. T. La, [REDACTED]
[REDACTED]
[REDACTED]
- [4] L. B. T. La, C. Leatherday, P. Qin, Y. K. Leong, K. J. Hayward, B. Jiang, and L.C. Zhang, "The interaction between encapsulated Gd_2O_3 particles and polymeric matrix: The mechanism of fracture and X-ray attenuation properties," *Colloids and Surfaces A: Physicochemical and Engineering Aspects*, vol. 535, pp. 175-183, 2017.

LIST OF ABBREVIATIONS

AOT: sodium di-2ethylhexyl sulfosuccinate
CPP: critical packing parameter
CTAB: cetyl trimethyl ammonium bromide
CTAC: cetyltrimethylammonium chloride
DDAB: didodecylammonium bromide
DGEBA: diglycidyl ether of bisphenol A
FTIR: fourier transform infrared spectroscopy
Gd(AA)₃: gadolinium acrylate
Gd-nanocomposite: Gd₂O₃ particulate epoxy composite
HBL: hydrophile- lipophile balance
IDPI: isophoronediiisocyanate
IEP: isoelectric point
NBR: Nitrile butadiene rubber
NPs: nanosized particles
NR: Natural rubber
O/W: oil in water emulsion
O-I composite: organic-inorganic composite
PEEK: poly ether ether ketone
PEG: polyethylene glycol
PVA: polyvinyl alcohol
SDS: Sodium ammonium dodecyl sulphate
SDS-Gd: milled Gd₂O₃ encapsulated in Sodium ammonium dodecyl sulphate surfactant
SEM: Scanning electron microscope
SPAN 80: sorbitan monooleate
TEM: Transmission electron microscopy
THF: Tetrahydrofuran
TX-100: p-tert octylphenylpolyoxyethylene ether
W/O: water in oil emulsion
XRD: X-ray powder diffraction

TABLE OF CONTENTS

DISCLAIMER	I
USE OF THESIS.....	III
ABSTRACT.....	V
ACKNOWLEDGEMENT	VII
LIST OF ABBREVIATIONS.....	XI
LIST OF FIGURES.....	XVII
LIST OF TABLE	XXI
LIST OF SYMBOLS.....	XXIII
CHAPTER 1: INTRODUCTION	1
1.1. Research background.....	1
1.2. Statement of research questions	3
1.3. The objectives of this research	4
1.4 Scope of the research.....	5
1.5. Research significance and innovation.....	5
CHAPTER 2:BACKGROUND AND LITERATURE REVIEW	7
2.1. Introduction.....	7
2.2. Gadolinium element- discovery, production, properties, and applications	7
2.3. Gadolinium- a potential “green” element for new radiation shielding material	9
2.4. The light weight particulate polymer composite - current commerciallead and non-lead-based materials for X-ray protection	13
2.5. Epoxy polymer-effective matrix for Gd-particulate composite and the factors influencing their mechanical performance.....	15
2.6. Nano and submicron scale particles-the importance and effect on composite’ properties	18
2.7. Processing strategies for nanocomposite synthesis	19
2.8. Discussion of conventional methods for preparation of nanosized particles.....	22
2.9. Particle surface modification.....	39
CHAPTER 3: RESEARCH METHODOLOGY	41
3.1. Materials and experimental testing methods.....	41
3.2. Experimental structure:.....	44
CHAPTER 4: X-RAY PROTECTION, SURFACECHEMISTRY AND RHEOLOGY OF BALL-MILLED SUBMICRON Gd ₂ O ₃ AQUEOUS SUSPENSION.....	49
4.1. Introduction	49

4.2. Materials and methods	51
4.3. Results and discussion	52
4.4. Conclusion.....	62
CHAPTER 5: A NOVEL APPROACH FOR THE PREPARATION OF NANOSIZED Gd ₂ O ₃ STRUCTURE: THE INFLUENCE OF SURFACE FORCE ON THE MORPHOLOGY OF BALL MILLED PARTICLES.....	65
5.1. Introduction	65
5.2. Materials and method.....	66
5.3. Result and discussion.....	68
5.4. Conclusion.....	76
CHAPTER 6: GREEN LIGHTWEIGHT LEAD-FREE Gd ₂ O ₃ /EPOXY NANOCOMPOSITES WITH PROMINENT X-RAY ATTENUATION PERFORMANCE	79
6.1. Introduction	79
6.2. Materials and method.....	80
6.3. Results and discussion	82
6.4. Conclusion.....	91
CHAPTER 7: THE INTERACTION BETWEEN ENCAPSULATED Gd ₂ O ₃ PARTICLES AND POLYMERIC MATRIX: THE MECHANISM OF FRACTURE AND X-RAY ATTENUATION PROPERTIES	93
7.1. Introduction	93
7.2. Materials and method.....	94
7.3. Results and discussion	97
7.4. Conclusion.....	107
CHAPTER 8: SUMMARY AND FUTURE WORK.....	109
8.1. Thesis Summary	109
8.2. Future work	111
REFERENCES.....	113
APPENDIX A: STANDARD OPERATION PROCEDURE OF ZETA POTENTIAL ANALAYSIS	133
APPENDIX B: X-RAY ATTENUATION EFFICIENCY OF SPECIMENS.....	139
APPENDIX C: X-RAY ATTENUATION EFFICIENCY OF Pb SHEETS.....	141
APPENDIX D: THE THICKNESS OF LEAD, WOOD, CONCRETE AND GLASS AT CORRESPONDING RADIATION ATTENUATION EFFICIENCY OF SPECIMENS....	143

APPENDIX E: WEIGHT- THICKNESS Gd_2O_3 /EPOXY NANOCOMPOSITE (g/cm^2) AT
DIFFERENT PARTICLE VOLUME FRACTIONS..... 145

LIST OF FIGURES

CHAPTER 1	1
CHAPTER 2	7
Figure 2.1. Gadolinium metal [31].....	8
Figure 2.2. Special application in medical area relating to special properties of Gd ₂ O ₃ nanoparticles [48].....	9
Figure 2.3. Electromagnetic spectrum chart with corresponding radiation applications and biological effects [51].....	9
Figure 2.4. The penetrating capacity of different types of radiation [54]	11
Figure 2.5. Comparison of the gaps between the ground energy level and the first excited state of the Gd and other rare-earth elements [65].....	13
Figure 2.6. The scale of things for nanometer definition [94].....	18
Figure 2.7. (A) Gold and (B) silver nanoparticles in different size in water [99].....	19
Figure 2.8. Scheme of in-situ and ex-situ method [101]	20
Figure 2.9. The SEM image of (A) the Gd(AA) ₃ synthesized particles and (B) the particulate rubber composites(the weight loading of Gd(AA) ₃ is 50wt%) [55].....	21
Figure 2.10. TEM micrographs of epoxy/modified-Gd ₂ O ₃ nanocomposite (10wt.-%) [7].....	21
Figure 2.11. Scheme of Top-Down and Bottom-Up routes to the preparation of nanosized particles (NPs) [101].....	23
Figure 2.12. Scheme of the stages of nucleation and growth for the preparation of monodispersed nano crystals in the framework of the La Mer model [97].....	25
Figure 2.13. Schematic of the synthetic procedure to (a) synthesize nanocrystals by high temperature solution-phase routes, (b) narrow nanocrystal size distribution by size-selective precipitation, (c) deposit nanocrystal dispersions that self-assemble [106]	26
Figure 2.14. Scheme of water-in-oil microemulsion [114]	29
Figure 2.15. Effect of molecular moieties and solution conditions on the CPP of a surfactant and the resulting range of possible surfactant aggregates in water or aqueous solution [112].	30
Figure 2.16. Schematic representation of synthesis of nanoparticles in microemulsions (a) by adding a reducing agent to a microemulsion, (b) by bubbling gas through a microemulsion and (c) using two microemulsions [113]	32
Figure 2.17. Processing routes to materials using sol-gel methods [3,125].....	34
Figure 2.18. The scheme of high energy ball milling [155]	38

Figure 2.19. Schematic representation of unstable and stable solid-liquid suspension systems under the influence of surface modification	40
CHAPTER 3	41
Figure 3.1. Specimen geometry based on ASTM D638-99 for tensile testing of plastics.	42
Figure 3.2. The geometry of Compact tension specimens.....	43
Figure 3.3. Scheme of experimental structure with objectives (Obj).....	47
CHAPTER 4	49
Figure 4.1. (A) The particle diameter of gadolinium oxide versus milling time at different ratios of Gd ₂ O ₃ :NaCl at d ₉₀ , and (B) The size distribution of gadolinium oxide for 70 minutes of milling at different Gd ₂ O ₃ :NaCl ratios.	54
Figure 4.2. SEM micrograph of premilled (A) and milled Gd ₂ O ₃ (B) obtained after 70 minutes of milling at a weight ratio of 1:1.5 of Gd ₂ O ₃ : NaCl	55
Figure 4.3 The zeta potential (ζ) -pH behaviour of a milled and cleaned Gd ₂ O ₃ suspension ...	56
Figure 4.4. The influence of solid volume fraction (ϕ_s) on the yield stress-pH of Gd ₂ O ₃ aqueous suspensions.....	57
Figure 4.5. The relationship of maximum yield stress ($\tau_{y,max}$) and solid volume fraction (ϕ_s) of Gd ₂ O ₃ suspension in log-log scale	58
Figure 4.6. The correlation between yield stress (τ_y) and the square of zeta potential (ζ^2).....	59
CHAPTER 5	65
Figure 5.1. SEM images of: (A) premilled Gd ₂ O ₃ , (B) ball-milled unmodified Gd ₂ O ₃ , and (C) and (D) the ball-milled modified Gd ₂ O ₃ under the effect of CTAB and SDS surfactants respectively.	69
Figure 5.2. Size distribution by frequency in volume (%) of unmodified and modified Gd ₂ O ₃ suspension.....	70
Figure 5.3. XRD patterns of ball milled Gd ₂ O ₃ particles under the effect of surfactants modified SDS, modified CTAB and unmodified milled, and commercial or premilled Gd ₂ O ₃ (99.99%)	71
Figure 5.4. (A) The zeta potential and (B) yield stress of milled Gd ₂ O ₃ suspension, describing the change in the surface charge and dispersed-agglomerated state of milled Gd ₂ O ₃ suspension.....	73
Figure 5.5. The relationship between yield stress and pH value of Gd ₂ O ₃ suspension.....	74
CHAPTER 6	79
Figure 6.1. Size distribution by frequency in volume (%) of pristine and synthesized Gd ₂ O ₃	83

Figure 6.2. SEM images to show the morphology of (A) unmilled and (B) milled and SDS-Gd ₂ O ₃	83
Figure 6.3. SEM images of Gd ₂ O ₃ /epoxy surface providing visible information of the dispersion of particles in epoxy matrix at different magnifications.....	84
Figure 6.4. Illustration of an inorganic particle surrounded by a strongly adsorbed layer of organic molecules of typically 1-2nm thickness (core shell particle).....	85
Figure 6.5. The Infrared spectra of pristine Gd ₂ O ₃ and SDS shell/Gd ₂ O ₃ core nanoparticles..	86
Figure 6.6. The plot of effective radiation attenuation and maximal primary beam energy (kVp) for different particle volume fraction values (ϕ_s) of Gd ₂ O ₃	88
Figure 6.7. Comparison of the weight per unit area at the same radiation attenuation efficiency of Gd ₂ O ₃ /epoxy composite ($\phi_s=0.14$, 8mm thickness) to conventional structural materials (concrete, wood, glass, and standard Pb sheeting) across a range of diagnostic beam energies	89
Figure 6.8. Comparison of the relative attenuation efficiency of Gd ₂ O ₃ -composite ($\phi_s=0.14$, 8 mm thickness) to a 0.5 mm Pb equivalence commercially available lead-free materials at different energy levels, with reference to a pure Pb standard.....	90
CHAPTER 7	93
Figure 7.1. Geometry of compact tension specimen.....	96
Figure 7.2. SEM morphologies of Gd ₂ O ₃ at: (A) unmilled, (B) milled and SDS conditions..	98
Figure 7.3. Schematic illustration of Gd nanoparticles surrounded by strongly adsorbed layer of organic molecules (core shell Gd ₂ O ₃ particles) and their FTIR spectra.....	99
Figure 7.4. The relationship between (a) tensile strength and (b) Young's modulus with the volume fraction of Gd ₂ O ₃ particles.	100
Figure 7.5. The fracture toughness of neat epoxy and its nanocomposites at different volume fractions	101
Figure 7.6. Fractograph of (A) neat epoxy matrix and (B, C, D, E) Gd nanoparticle ($\phi_s=0.08$) epoxy composite at different magnifications.	102
Figure 7.7. Mechanism of crack growth paths for organic encapsulated nano Gd ₂ O ₃ particles in epoxy resin.	103
Figure 7.8. The relationship between X-ray attenuation coefficient (A) and volume fraction (ϕ_s) for the Gd-filled composites with (a) 8 mm and (b) 16 mm thicknesses.....	104
Figure 7.9. The relationship between X-ray attenuation and beam energy (E) at different volume fraction (ϕ_s).....	105

Figure 7.10. (A) The effective radiation attenuation of particulate composite ($\phi_s=0.08$, $\phi_s=0.1$) at different thicknesses and lead equivalences, and (B) the comparison of weight per unit area at the same radiation attenuation proficiency between Gd_2O_3 /epoxy composite ($\phi_s =0.1$, 16 mm thickness) and some convenient materials sheeting across a range of diagnostic beam energies 107

CHAPTER 8 109

LIST OF TABLE

CHAPTER 1	
Table 1.1. Comparison of selected general properties of frequently used organic polymers and inorganic metals or metallic substances [2].....	1
CHAPTER 2	7
Table 2.1. Comparison of potential metallic elements for radiation shielding properties through thermal neutron capture cross sections data and atomic numbers (2013)	12
Table 2.2. A comparison of the pros and cons of in-situ and ex-situ routes	22
Table 2.3. Summary table with the control parameters of previous research pieces using classical coprecipitation approach.....	27
Table 2.4. Microemulsion methods for synthesis of nanoparticles.....	31
Table 2.5. Gadolinium compound preparation using water in oil microemulsion method.....	33
Table 2.6. Gadolinium compounds preparation using water in sol-gel method	35
CHAPTER 3	41
CHAPTER 4	49
Table 4.1. The comparison of weight-thickness (g/cm^2) of Gd_2O_3 suspension ($\phi_s \sim 0.082$) and other commercial X-ray protective materials at the equivalent effective attenuation capacity.....	62
CHAPTER 5	65
CHAPTER 6	79
Table 6.1. The densities correspondent to Gd-composite at different volume fractions (ϕ_s).....	87
Table 6.2. A comparison of weight per unit area (g/mm^2) at 0.5 mm Pb equivalence	91
CHAPTER 7	93
CHAPTER 8	109

LIST OF SYMBOLS

- ϕ_s : volume fraction of solids (dimensionless)
- τ_y : yield stress (dimensionless)
- ζ_{crit} : critical zeta potential (dimensionless)
- ζ : zeta potential (dimensionless)
- W : Width (m or mm)
- T : X- ray transmission (dimensionless)
- T : thickness (m or mm)
- S : the value displaying on viscometer screen (%)
- P : is the load applied (N)
- L : Length (mm)
- K_{sv} : vane constant (m^3)
- K_{IC} : the plane strain critical stress concentration factor ($Mpa.m^{1/2}$)
- K : the air kerma (kinetic energy released per unit mass of air) (Gy)
- k : Debye parameter (dimensionless)
- G_{IC} : the critical strain energy release rate ($J.m^{-2}$)
- G : Gauge length (mm)
- ϵ_w : permittivity of water (dimensionless)
- E : Young's modulus (MPa)
- Do : the surface distance between two particles (m)
- d_{10} , d_{50} , d_{90} : the particle diameter (μm) in the cumulative distribution at 10 vol.%, 50 vol.%, 90 vol.%
- D : surface separation distance between the interacting particles
- A_{121} : Hamaker constant of the particle in water (zj)
- A : X-ray absorption proficiency (dimensionless)
- a : particle radius (m)
- ν : Poisson's ratio

CHAPTER 1: INTRODUCTION

1.1. Research background

Hybrid organic and inorganic materials have been manufactured and in use since the 1950s. Their desirable properties result from combining some distinct characteristics of two or more components [1]. Individual types of inorganic and organic matters show typical properties that are a trade-off between their positive and negative characteristics. As can be seen from Table 1.1 for each characteristic, if one performs well, the other performs poorly and vice versa. The goal of combining both classes of these materials into hybrids is to develop new materials that have the advantages of both. One of the common ways to prepare a hybrid material is a dispersion of micron- or nanosized inorganic particles in an organic matrix. For example, instead of an expensive laminated structure of metallic compounds such as silver oxides or gold, only a small amount of the particles of these substances can be dispersed in polymers to generate O-I materials with the same functional characteristics [2].

Table 1.1. Comparison of selected general properties of frequently used organic polymers and inorganic metals or metallic substances [2]

Property	Polymers or organic materials	Metals or inorganic substances
Density	Low	High
Optical transparency	High	Low
Electric insulation ability	High	Low
Thermal insulation ability	High	Low
Melting temperature	Low ⁺	High
Corrosion resistance	High	Low
Thermal stability	Low	High
Fire resistance	Low	High
Radiation resistance	Low ⁺	High

In the 1980s, the investigation of nanotechnologies led to the development of particulate hybrid organic-inorganic (O-I) nanocomposites in which the miniaturisation of the inorganic fillers in a polymer could improve the properties of hybrid products[3,4]. Particulate hybrid nanocomposites are divided into two main types, namely reinforced and functional polymer

nanocomposites. Reinforced nanocomposites involving the dispersion of inorganic nanosized particles of titanium compound, clay, calcium carbonate, carbon and glass fiber in different polymer matrices have been used in construction, cryogenic applications, defense, automobile and even in aircraft and aerospace areas [5,6]. Additionally, other metallic compounds with special properties are also combined with polymer matrices to create customized functional particulate nanocomposites. For example, a polyvinyl alcohol (PVA) polymer with fluorescent enhancement from the dispersion of gold nanoparticles provides a contrast in scanning probe microscopy and Raman spectroscopy or a molecular beacon for biomolecular recognition in sensing applications. Another example includes lead compounds/rubber composites that were synthesized to provide radiation shielding properties [7-9].

In this research, a new kind of functional particulate nanocomposite will be synthesized from dispersion of synthesized gadolinium oxide nanoparticles into an epoxy matrix. Because of a special electron configuration, this element can absorb X-ray radiation with high energy and a high degree of penetration. Although metallic lead material or lead/rubber hybrid composites conventionally were used as effective radiation shielding materials in medical practices, compared to gadolinium, it still has limitations on functional properties as well as being toxic [7-9]. Recently, there has been a recognition among manufacturers and users of a trade-off between the economic, health and environmental benefits of using Pb-free X-ray protection aprons that are composed of less toxic metallic powder than Pb imbedded into polymer. This recognition is reflected in an increasing demand for these “green” aprons despite the higher price of the products [10-12]. In this research, gadolinium is proposed as an element to replace Pb for “green” radiation protection. Combination Gd particles with a polymer can vary the mechanical performances of hybrid material from hard and stiffness to flexibility (rubber-like) for the multiple uses. Furthermore, this hopefully reduces the amount of gadolinium material required, and this reduces the weight of the product. Additionally, an effective and inexpensive method is proposed to decrease the cost of preparation.

The organic matrix of gadolinium/polymer nanocomposites may come from many kinds of polymer matrices such as rubber, polyvinyl alcohol (PVA), polyamide, and epoxy resin. In this work, epoxy resin, a kind of thermosetting polymer, will be used as a matrix of nanocomposite. Different kinds of epoxy polymers are effectively employed to disperse inorganic particles to create particulate composites for many applications. For example, nanosized particles such as Al_2O_3 , SiO_2 , ZnO and BeO , SiC , AlN , Si_3N_4 are dispersed in epoxy to prepare thermally conductive but electrically insulative adhesives or composites [13-

15]. Silica, mica, and calcium carbonate were investigated and administrated as fillers to improve the dielectric constant of epoxy thin film composites used in capacitor applications in the electronic packing industry [16]. A silver/epoxy composite has been proposed as a potential electrical conductive adhesive [15]. Graphene platelet reinforced epoxy has been developed as high thermal stability material [17-20].

Epoxy resins have valuable characteristics that make them an outstanding matrix such as low cost, low density, effective moisture resistance, chemical, corrosion and heat resistance, high electrical insulation, and good optic properties. More importantly, cured epoxy resin can vary from malleable, ductile, and tough to hard, strong, and brittle matrices. These performances are obtained by controlling the chemical structure of the epoxy oligomer and the curing agent [5,21,22]. Finally, it possesses exceptional processing characteristics such as an absence of byproducts or volatiles during curing reactions, slow shrinkage on cure, curing over a wide temperature range and the control of the degree of cross-linking [5,22]. As a result, epoxy formulations have been utilized in technical applications including protective coatings, adhesives, and as a matrix resins for high strength composites [23]. It is also used to replace metal, wood, and other traditional materials in industrial tooling applications to produce molds, master models, laminates, and castings. Due to improved manufacturing efficiency, the overall cost is lowered and the lead-time is shortened for many industrial processes [16,21,24]. Due to these properties, epoxy resin is chosen in this study as the matrix for an exploration of the properties of nanosized gadolinium oxide particle/ epoxy composite.

1.2. Statement of research questions

1.2.1. Research problem

Nanocomposites are not simply physical mixtures which reflect the sum of the individual contributions of the performances of the constituent phases, but their important features are formed by the interaction between them [1,4,25]. Inhomogeneous dispersion can cause poor performance of the final product. The local aggregation and precipitation of the high loading content of the particle phase in continuous phases are usually found in poor disperse composite. Homogeneous dispersion is defined through two parameters: optimal internal interaction and chemical surface compatibility between two phases. To understand the research problem, some definitions and principles of phenomenon will be presented below.

Reducing the size of particles to nanoscale can theoretically increase homodispersion. However, it also increases the internal interaction surface area between the solid and liquid

phases and so increases the risk of particle agglomeration in fabrication process due to poor wettability and chemical compatibility between them [2].

The dispersability of the solid inorganic phase in a high viscous liquid organic phase is explained by wettability which may cause a thermodynamically stable or unstable solid-liquid suspension system. Wetting is the ability of a liquid to maintain contact with a solid surface resulting from intermolecular interactions when they are mixed together. It plays an important role in bonding or the adherence of two different phase materials in one heterogeneous mixture. The degree of wetting is determined by the chemical homogeneity between the particles in the solid phase and the matrix in the liquid phase[2].

A novel methodology of rare earth Gd_2O_3 /polymer nanocomposites preparation is developed to address the disadvantages of the previous methods. Three main questions are covered:

1. How can nanoparticles of gadolinium oxide (Gd_2O_3) be synthesized using a convenient and inexpensive method?
2. How can the dispersion of synthesized particles in the epoxy matrix be improved?
3. How can the X-ray shielding and mechanical properties of the synthesized Gd/epoxy nano composite be characterized?

1.2.2 Research hypotheses

- Unlike current methods using available nanoparticle compounds, this research will start from the early stage of nanoparticle preparation before proceeding to the final stage of nanocomposite synthesis. Conducting these processes sequentially will allow better control of particle dispersion in the polymer matrix and reduce the cost of the process.
- The miniaturization of the dispersed phase to nanoscale improves the total interface area between the two phases leading to markedly improved mechanical and functional performance.
- The selection of suitable particle surfactant for particle surface-modification is expected to enhance chemical compatibility between two phases effectively.

1.3. The objectives of this research

The primary purpose of this research is to develop a novel methodology for the synthesis of a new type of organic/inorganic nanocomposite with high radiation shielding properties

using Gadolinium compounds as nanosized fillers in an epoxy resin matrix. Other characteristics such as mechanical, chemical, and especially X-ray radiation attenuation properties are to be investigated. The research has the following specific objectives:

- 1) Identify the relationship between synthesis conditions and the Gd_2O_3 particle size and geometry.
- 2) Determine the effect of interface compatibility and the dispersion of Gd compound particles in continuous phase (water and epoxy) on material properties.
- 3) Investigate the relationship between X-ray protective properties and mechanical performance.
- 4) Evaluate the synthesized nanocomposite as a “green”, lightweight, Pb-free material for X-ray protection.

1.4 Scope of the research

To eliminate irrelevancies to the identified objectives and the problems, the scope of the research was limited as follows:

- The study was limited to using only a commercial epoxy system ($d = 1.09\text{g/ml}$) as a matrix of nanocomposite from Struers supplier. Cured material is synthesized from bisphenol A (epichlorhydrin) epoxy resin (number average molecular weight ≤ 700 , $d = 1.1\text{g/ml}$) cured by Triethylenetetramine hardener ($d = 0.98\text{g/ml}$).
- The study used bulky gadolinium oxide (Gd_2O_3) available on the market as a precursor and for further processing.
- The strategy for blending two phases together including ex-situ and in-situ; however, this research just used ex-situ method to avoid unexpected reactions or side products during nanocomposite processing.

1.5. Research significance and innovation.

This research will advance knowledge in the area of hybrid nanocomposite preparation. The current methods are problematic due to inefficient process control, low yield of particle content, and the use of large amounts of organic solvents for interface improvement. By addressing the disadvantages of the existing approaches, a novel methodology this research is able to develop fundamental knowledge regarding ways to combine ideal functional properties with outstanding mechanical performance for particulate nanocomposites. As a

result, many new types of functional polymer/metal nanocomposites that might be used by the manufacturing, medical, mining, transport, and information and communications industries will be developed.

The study also provides essential information for developing an inexpensive and effective method to produce the nanosized gadolinium oxide particles which are employed in many practical applications, particularly in medical practice. More importantly, these consequent processes provide an effective and low cost approach for Gd-nanocomposite preparation that represents a new type of “green” radiation shielding material. These materials will be developed to protect people from dangerous radiation emanated from radioactive medical practices, mining, nuclear reactors, spatial and atomic research, and even the natural environment.

Being is one of 5 countries (China, USA, Brazil, India, Australia) occupying main mining with reserves annually the accumulative amount of 400 tones pure Gadolinium for industry and medical application, Australia takes obviously advantages in commercializing, developing and manufacturing this new “green” material [26-28].

CHAPTER 2: BACKGROUND AND LITERATURE REVIEW

At the author's request, Chapter 2 has been omitted from this version of the thesis.

CHAPTER 3: RESEARCH METHODOLOGY

3.1. Materials and experimental testing methods

3.1.1. Precursor gadolinium (III) oxide materials

Two precursor gadolinium (III) oxide (Gd_2O_3) powders with a purity of 99.99% at different diameter were used in this research. The first product purchased from Alfa Aesar (United Kingdom) had a size distribution of $d_{10}=0.28\mu m$, $d_{50}=4.34\mu m$ and $d_{90}=10.6\mu m$. The second one supplied by Sun Chemical Technology (Shanghai) Co., China had a size distribution of $d_{10}=0.26\mu m$, $d_{50}=5.50\mu m$ and $d_{90}=29.9\mu m$.

3.1.2. Size reduction and surface study

A high-energy SPEX8000 mixer/mill with hardened steel balls (12.5 mm diameter) at room temperature was used for Gd_2O_3 particle size reduction. Size distribution depends on the weight ratio between additives and powder, and milling time.

The zeta potential-pH behavior of mill Gd_2O_3 particles in water was characterized using a Colloidal Dynamic ZetaProbe operated in the potentiometric titration mode using 0.7 M KOH or 0.7 M HNO_3 solutions as the titrants.

The (static) yield stress-pH behavior was characterized using a Brookfield vane viscometer. At each step change of pH, the sample was agitated vigorously with a spatula for at least 15 minutes before pH and yield stress were measured. The maximum torque applied on a rotating (0.4 rpm) vane submerged in the colloid was transformed to the corresponding yield stress

$$\tau = \frac{S\%}{100} \times \frac{\text{Viscometer constant}}{K_{sv}} \quad (3.1)$$

K_{sv} (m^3): vane constant Vane 74 KSV= $7.5 \times 10^{-7} m^3$

Viscometer constant of LVDVII Pro= $6.73 \times 10^{-5} NM$

Viscometer constant of RVDV-II+ Pro= $0.7187 \times 10^{-3} NM$

τ (Pa): Yield stress

S (%): the value displaying on viscometer screen

3.1.3. The morphology of synthesized nanoparticles, their dispersion in cured epoxy and fractography of Gd-nanocomposite

The size distribution of synthesized Gd_2O_3 particles was determined using a Malvern Mastersizer Microplus Particle Size Analyzer. Their morphology was also characterized by a scanning electron microscope (SEM) (a Zeiss 1555 VPSEM).

The diffuse map, geometry and size of dispersed particles and the fracture surface of synthesized nanocomposite were also observed through the above SEM. This provided information on the effect of homogeneous and mono dispersion on functional properties and mechanical performance.

3.1.4. Chemical characterization of encapsulated nanofillers

The chemical structure of synthesized Gd-nanoparticles was investigated using Fourier transform infrared spectroscopy (FTIR) (Perkin Elmer) and X-ray diffraction (XRD) using a PANalytical EMPYREAN diffractometer with $Co\ K\alpha$ radiation ($\lambda = 0.1789\text{nm}$).

3.1.5. Mechanical testing method

An Instron 5982 universal testing machine and its extensometer were employed to evaluate the mechanical properties of the Gd_2O_3 particulate composite at different solid volume fractions (ϕ_s) of 0, 0.04, 0.06, 0.08, 0.1, 0.12, 0.14.

Five dumb-bell specimens (Figure 3.1), based on the ASTM standard D638-02a specification of a gauge length of 50 mm and constant thickness of 5 ± 1 mm, were prepared for each composite composition. The crosshead rate of 0.5 mm/min was used for tensile mechanical testing. The elastic deformation of the composite under load (Young's modulus) was estimated from the gradient of the stress-strain curve. All the mechanical properties reported in this work were averaged from at least four individual tests.

W – Width of narrow section	13 mm
L – Length of narrow section	57 mm
WO – Width overall, min	19 mm
LO – Length overall, min	165 mm
G – Gage length	50 mm
D – Distance between grips	115 mm
R – Radius of fillet	76 mm
T – thickness	4 mm

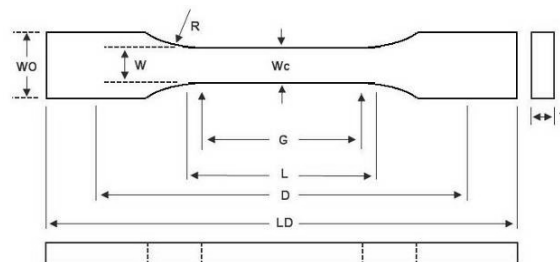


Figure 3.1. Specimen geometry based on ASTM D638-99 for tensile testing of plastics.

Five compact tension specimens (Figure 3.2) were also prepared for each composite composition to determine their fracture toughness. Again, a crosshead rate of 0.5 mm/min was employed. The fracture toughness characterizes the material's resistance to brittle fracture in the presence of a crack. Two important parameters were calculated from the tests, i.e. the plane strain critical stress concentration factor (K_{IC}) and the critical strain energy release rate (G_{IC}), according to ASTM D 5045-99. The compact tension specimen configuration is shown in Figure.3.2. A pre-notch crack made by a band saw should be followed by tapping to create a pop up crack for fracture toughness measurement. The results should be validated by using stress-strain graphs as detailed by the standard. The razor crack length was in the range of $0.45 < a/W < 0.55$. The K_{IC} is given by:

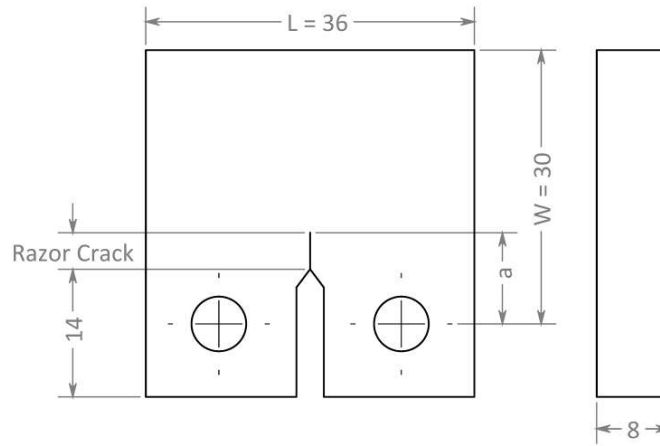


Figure 3.2. The geometry of Compact tension specimens

$$K_{IC} = \frac{P \cdot F(x)}{T \cdot W} \quad (3.2)$$

where P is the load applied, T, W are the thickness and the width of specimens. F(x) is a function of $x = \frac{a}{W}$ and is defined as follows.

$$F(x) = \frac{(2+x) \cdot (0.866 + 4.64x - 13.32x^2 + 14.72x^3 - 5.6x^4)}{(1-x)^{3/2}} \quad (3.3)$$

The plane strain energy release rate (G_{IC}) can be calculated as follows,

$$G_{IC} = \frac{(1 - \nu^2) \cdot K_{IC}^2}{E} \quad (3.4)$$

E : Young's modulus

ν : Poisson ratio

3.1.6. Radiation shielding property

The attenuation capacity of specimens was tested at Royal Perth Hospital with beams of six different energies from 60 to 120kVp, the common diagnostic radiographic region. The photon beams from an X-ray tube source of a Mobile DR X-ray unit (GE Optima XR220AMX) were emitted for 25 seconds at a current of 100 mA to suspensions as a radiation shielding screen. The radiation transmitted through samples was collected, recorded and analyzed using a free air chamber of a Non-invasive X-ray Beam Analyser (Unfors Xi R/F & MAM). In this study, the broad beam geometry of a DIN 6857 Standard test method was used: the distance from focal spot to chamber was one metre, and the sample sheets were located directly in front of this indicator. This geometry generates a more accurate attenuation measure because it is based on the total radiation reaching the chamber (contributed by penetrating primary and scattered radiation through materials), and the fluorescence generated by the sample itself [10,70]. The attenuation, A , achieved by the constant thickness Gd-composite at different particle volume fractions at different X-ray energies was defined as follows:

$$A(\phi_s) = \frac{K(0) - K(\phi_s)}{K(0)} \quad (3.5)$$

Where K is a quantity parameter designed for X-ray shielding calculations called air kerma (kineticenergy released per unit mass of air (grays (Gy))). The values of $K(0)$ and $K(\phi_s)$ are the air kerma without shielding, and shielded by specimens with different particle volume fractions, at X-ray energy levels

3.2. Experimental structure:

Outlining the overall experimental structure of the research project was introduced in Figure 3.3. This part then briefly summarizes the works undertaken for each objective. All the

projects were recorded and discussed in journal articles, which are included in Chapters 4 to 7.

Task 1 was achieved in peer-reviewed journal articles included here as Chapters 4 and 5. Chapter 4 provided the relationship between particle size and milling time and the weight ratios of additive NaCl and Gd₂O₃ precursors. The research also studied the surface characteristics of milled submicronized Gd₂O₃ in aqueous solution. The dispersed-flocculated behavior of milled submicronized Gd₂O₃ aqueous slurries was investigated via yield stress and zeta potential versus pH value techniques to stabilize the dispersion. Then well dispersed synthesized Gd aqueous suspensions at different volume fractions at a constant thickness were prepared for initial investigations of radiation attenuation performance. Based on the previous knowledge from Chapter 4, the effect of inter-particle forces arising from adsorbed typical cationic and anionic surfactants on the morphology of ball milled Gd₂O₃ was researched in Chapter 5. The experimental outcomes were interpreted in terms of the stabilization and interaction mechanisms of fine washed Gd₂O₃ particles (size diameter <1μm) in an aqueous medium under the variation of surface forces arising from adsorbed surfactant. Two different kinds of surfactants including anionic (sodium dodecyl sulfate (SDS)) and cationic (cetyl trimethyl ammonium bromide (CTAB)) capping agents were used for this study. The results recorded in Chapter 5 proved that the adsorbed organic SDS shell prevented the fine particles from re-welding during the dispersing, annealing route for both nanoparticle preparation and surface modification for particulate composite preparation.

Task 2 was achieved in peer-reviewed journal articles included here as Chapters 6 and 7. In these experiments, nanoscale SDS surface-modified Gd₂O₃ particles were dispersed in epoxy matrix to produce particulate Gd₂O₃ epoxy nanocomposite (Gd nanocomposite). The adsorption of sodium dodecyl sulphate (SDS) surfactant on the surface of ultrafine ball milled Gd₂O₃ based on the effect of inter-particle forces reduces their agglomeration and aggregation in nanoparticle preparation and dispersion in the polymer matrix, thereby improving the radiation attenuation property of this material per unit area. The article included as Chapter 6 explored the relationship between solid volume fractions at a constant thickness of 8 mm and the X-ray protective performance of Gd₂O₃/epoxy nanocomposite. The X-ray protective performance versus weight per unit area of these specimens was also evaluated through different levels of X-ray protection in other materials such as concrete, glass, wood and especially other commercial lightweight “lead-free” products.

Work reported in Chapter 7 focused more on the dependence of the mechanical properties (fracture toughness, Young's modulus and tensile stress) of particulate Gd-nanocomposite on different particle volume fractions. The amount of synthesized Gd_2O_3 particles (the optimal value of particle volume fraction ($\phi_{s(opt)}$)) in pure epoxy that was required to increase the fracture toughness (K_{IC}) value maximally was recorded. An examination of the microstructure of the fracture surface at this $\phi_{s(opt)}$ was employed to observe the dispersion of the filler in the matrix. This is a plausible mechanism for explaining the improved toughness. At a constant value of the volume fraction, the X-ray attenuation proficiency depends on the thickness of material. Based on the mechanical testing result, filled composite at $\phi_{s(opt)}$ at 8 mm thickness and 16 mm thickness was fabricated to investigate X-ray attenuation proficiency. Then, the X-ray protective performance versus weight per unit area of specimens with $\phi_{s(opt)}$ at different thicknesses was compared to that of wood, glass, concrete, and current commercial non-lead products.

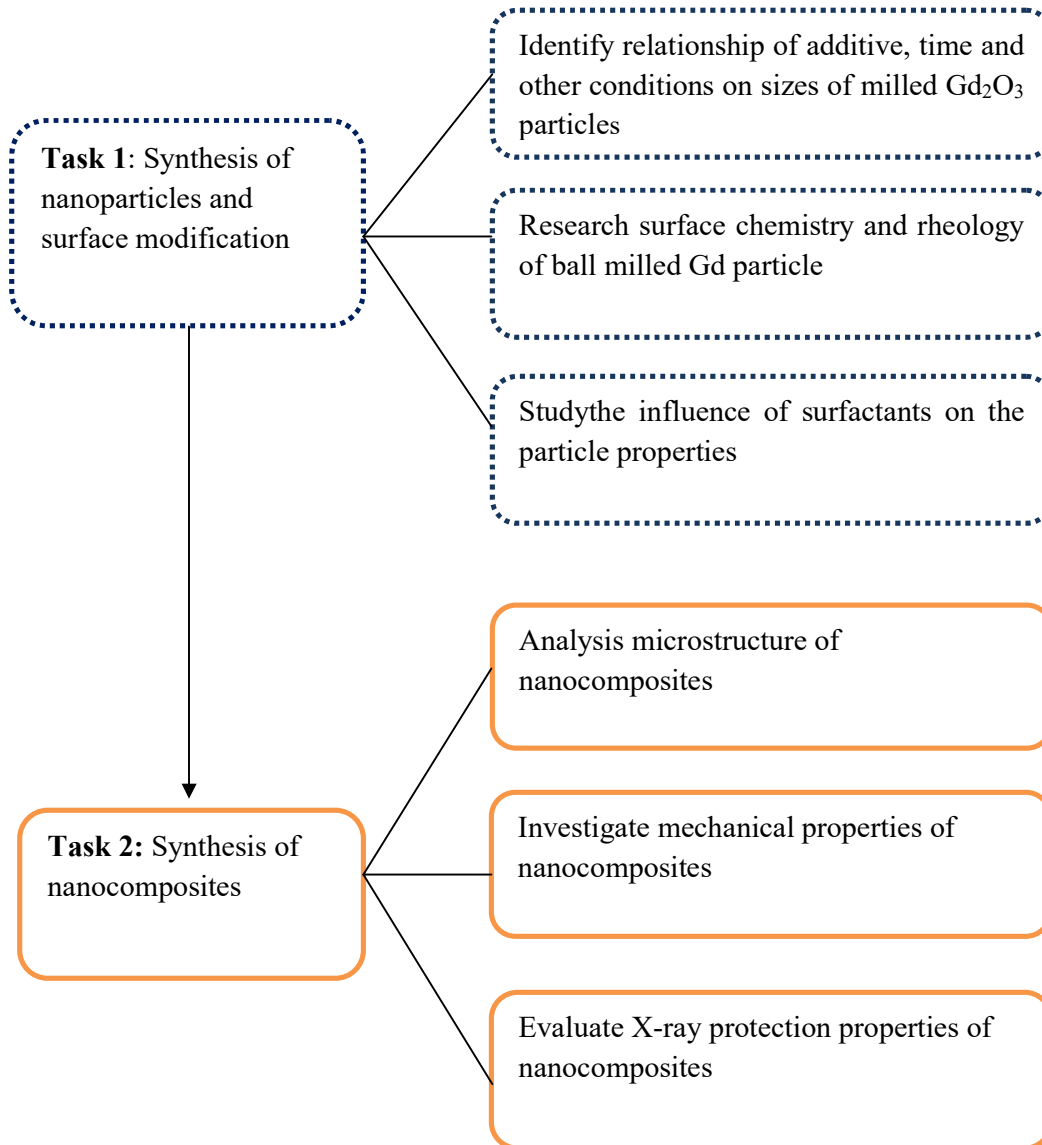


Figure 3.3. Scheme of experimental structure with tasks and sub objectives

CHAPTER 4: X-RAY PROTECTION, SURFACE CHEMISTRY AND RHEOLOGY OF BALL-MILLED SUBMICRON Gd₂O₃ AQUEOUS SUSPENSION

Due to copyright reasons, Chapter 4 has been omitted from this version of the thesis.

Chapter 4 has been published as:

La, L. B. T., Leong, Y.-K., Leatherday, C., Au, P. I., Hayward, K. J., & Zhang, L.-C. (2016). X-ray protection, surface chemistry and rheology of ball-milled submicron Gd₂O₃ aqueous suspension. *Colloids and Surfaces A: Physicochemical and Engineering Aspects*, 501(Supplement C), 75-82. doi: [10.1016/j.colsurfa.2016.04.058](https://doi.org/10.1016/j.colsurfa.2016.04.058)

The green open access version of the journal article is available [here](#).

CHAPTER 5: A NOVEL APPROACH FOR THE PREPARATION OF NANOSIZED Gd₂O₃ STRUCTURE: THE INFLUENCE OF SURFACE FORCE ON THE MORPHOLOGY OF BALL MILLED PARTICLES

Due to copyright reasons, Chapter 5 has been omitted from this version of the thesis.

Chapter 5 has been published as:

La, L. B. T., Leong, Y.-K., Watts, H. P., Au, P.-I., Hayward, K. J., & Zhang, L.-C. (2016). A novel approach for the preparation of nanosized Gd₂O₃ structure: The influence of surface force on the morphology of ball milled particles. *Colloids and Surfaces A: Physicochemical and Engineering Aspects*, 506(Supplement C), 13-19. doi: [10.1016/j.colsurfa.2016.06.005](https://doi.org/10.1016/j.colsurfa.2016.06.005)

The green open access version of the journal article is available [here](#).

**CHAPTER 6: GREEN LIGHTWEIGHT LEAD-FREE GD_2O_3 /EPOXY
NANOCOMPOSITES WITH PROMINENT X-RAY
ATTENUATION
PERFORMANCE**

At the author's request, Chapter 6 has been omitted from this version of the thesis.

CHAPTER 7: THE INTERACTION BETWEEN ENCAPSULATED Gd₂O₃ PARTICLES AND POLYMERIC MATRIX: THE MECHANISM OF FRACTURE AND X-RAY ATTENUATION PROPERTIES

Due to copyright reasons, Chapter 7 has been omitted from this version of the thesis.

Chapter 7 has been published as:

La, L. B. T., Leatherday, C., Qin, P., Leong, Y.-K., Hayward, K. J., Jiang, B., & Zhang, L.-C. (2017). The interaction between encapsulated Gd₂O₃ particles and polymeric matrix: The mechanism of fracture and X-ray attenuation properties. *Colloids and Surfaces A: Physicochemical and Engineering Aspects*, 535(Supplement C), 175-183. doi: <https://doi.org/10.1016/j.colsurfa.2017.09.038>
doi: [10.1016/j.colsurfa.2017.09.038](https://doi.org/10.1016/j.colsurfa.2017.09.038)

The green open access version of the journal article is available [here](#).

CHAPTER 8: SUMMARY AND FUTURE WORK

8.1. Thesis Summary

X-ray protective garments are typically comprised of lead-based materials, which are toxic to both people and the environment. Developing alternative lightweight radiation shielding materials is a priority for protecting people working with radiation. Gadolinium, with an electron configuration typical of radiation shielding elements, is proposed as a non-toxic replacement for lead. This study has provided new insights into the potential for a gadolinium suspension for replacing lead and proposes an effective preparation method. Inexpensive coarse Gd_2O_3 powder being 10- 15 times less expensive than nano one is employed as a starting material. Additionally, cheap and simple ball milling method are employed then, so the total cost of processing reduce considerably.

Firstly, submicron Gd_2O_3 particles with a size distribution of $d_{10} \sim 0.23$, $d_{50} \sim 0.38$ and $d_{90} \sim 0.8 \mu m$ are generated through a conventional and cost-effective ball milling method over 70 minutes with the mechanical support of a NaCl additive (1:1.5 Gd_2O_3 :NaCl). The dispersed-flocculated behaviour of Gd_2O_3 and thus the uniformity of suspension is determined by pH and the solid volume fraction. Flocculation or domination of the attractive particle force of Gd_2O_3 in an aqueous medium is investigated in the pH range from 9 to 12.5, in which maximum flocculation occurred at pH of 11. The point of dispersed-flocculated transition or the balanced state of attractive and repulsive forces in the slurry, which determines the stable dispersion of Gd_2O_3 aqueous suspensions, is about pH 9. Flocculated performance of the given particles is also affected by the solid volume fraction (ϕ_s) which strongly depends on its physical properties, such as the size, shape, and nature of the particles. Compared with other metal oxides at similar particle size, van der Waals attractive force of Gd_2O_3 particles in suspensions are unusually sensitive to the change of the volume fraction. This is due to the large variation in the shape and nature of the particles as characterized by the Hamaker constant. Based on the above information, the uniformly dispersed Gd_2O_3 aqueous suspensions prepared in the next stage provides the highly effective X-ray radiation shielding performance is required for a potential non-Pb based radiation attenuator.

This study also investigate the effect of inter-particle forces arising from adsorbed typical cationic and anionic surfactants on the morphology of ball milled gadolinium oxide (Gd_2O_3) for nano particle preparation and surface modification. The experimental outcomes are

interpreted in terms of the stabilization and interaction mechanisms of fine washed Gd_2O_3 particles (size diameter $<1\mu m$) in an aqueous medium under the variation of surface forces arising from adsorbed surfactant. After ball milling and washing, the point of zero charge or isoelectric point (IEP) of Gd_2O_3 particles suspension is at pH 11 where its maximum yield stress is observed. Because of hydrophobic interaction, the maximum yield stress of the Gd aqueous suspension increases by 30 times as the sodium dodecyl sulfate (SDS) is adsorbed on the particle surface and its IEP shifts slightly to a lower pH. Using cetyl trimethyl ammonium bromide (CTAB), the yield stress also increases by a much smaller extent (three times) and shifts to a higher pH of ~ 12.5 . Without surfactants, the microstructure of dried Gd_2O_3 displays the coarse particles of various shapes, i.e. rod, spherical, and cubic shapes. This indicates that the milled particles remain agglomerated in dispersion. In the presence of adsorbed anionic SDS, the particles are refined together with numerous 2D nanowire or nano-rod particles at pH ~ 8 . In contrast, coarser particles with absence of nano-rods are found when cationic CTAB is used to modify the Gd_2O_3 surface at a pH of about 12.5. The SDS-modified suspension exhibits a much higher yield stress, which results from finer particles in suspension. This is invoked from an organic shell formed by the high adsorbability of negatively charged heads of SDS into the bare positive charge density of the particle.

The adsorption of sodium dodecyl sulphate (SDS) surfactant on the surface of ultrafine ball milled Gd_2O_3 based on the effect of inter-particle forces reduces the agglomeration and aggregation in nanoparticle preparation and dispersion in the polymer matrix, thereby improving the attenuation property of this material per unit area. The relationship between X-ray attenuation of the synthesized particulate / epoxy composite and the particle volume fraction is investigated as follows: While a 8 mm thickness of Gd-nanocomposite with volume fractions (ϕ_s) of 0.10, 0.12, and 0.14 can reduce transmitted X-ray intensity by about 93-99%, a 16 mm composite thickness ($\phi_s=0.12$) can achieve more than 99% protection in the energy range of 60-120kVp. These specimens show comparable attenuation efficiency with 0.25, 0.35, 0.5, and 1 mm thickness of pure lead sheets that are normally used for radiology protection. The weight per unit area of Gd-nanocomposite ($\phi_s=0.14$, 8 mm thickness) is 6-20 times lighter than concrete, glass, and wood at the same attenuation performance (97-99% attenuation). The X-ray protective performance vs weight per unit area of this specimen is also evaluated through other commercial lightweight “lead-free” products. This specimen, with 36-48% less weight, shows better attenuation proficiency than 3 other commercial non-Pb composite products in the energy range above 73kVp.

The relationship between the quantities of synthesized core shell Gd_2O_3 added to epoxy matrix and the mechanical and X-ray attenuation properties of particulate epoxy composite is studied in this research. As a result, an optimal geometric design of non-lead-based X-ray protective material with reasonable weight per volume unit was prepared. A plateau with a 28-30% increment of fracture toughness (K_{IC}) value was observed with the addition of 0.08 to 0.1 volume fraction (ϕ_v) of Gd_2O_3 particles in pure epoxy. The same quantity of particles also optimally raises the critical strain energy release and the modulus of the epoxy about 22-24% and 18-25% respectively. An examination of the microstructure of the fracture surface shows relatively uniform nanoparticle dispersion, which is a plausible mechanism for explaining the improved toughness. The improved nanoparticle dispersion in the matrix enhanced both the mechanical and functional properties of the epoxy composite. A 1.6 cm thick sheet of fabricated filled composite at volume fractions of 0.08 and 0.1 can shield more than 95% (0.5 mm Pb equivalence) and 99% (1 mm Pb equivalence) of irradiated X-ray beam. At the same X-ray attenuation (99% attenuation), the specimen is 7, 8.5, and 16 times lighter than wood, glass, and concrete respectively. The composite at 0.5 mm Pb-equivalence also has 4.5-19.4% less weight per unit area than current commercial non-lead products.

This research successfully provides an optimal design and preparation process for a new “green” material for radiation shielding.

8.2. Future work

A Gd atom is both a good X-ray shielding material and a thermal neutron absorption material. This research has now shown that Gd also possesses excellent X-ray shielding properties. The high-energy neutron shielding properties of this material will be evaluated in the future.

Additionally, depending upon the nature of the applications, it is possible to change the Gd-epoxy from being stiff to being elastomeric by tailoring the structure of the epoxy and the crosslinking agent [78-80]. The material in this research is rigid but it is just pre-commercial radiation shielding material, so the elasticity of the materials will be an area of future research to commercialize products.

For potential applications, the Gd- epoxy formulation can be used as a coating or an adhesive to improve the X-ray attenuation proficiency of permanent structures such as the walls, floors, and rooves of a radiographic x-ray room and other items in this room. It also can be used as a portable X-ray shielding screen or the shell structure of an X-ray radiator to

restrict undesirable radiation or radiation leakage. In addition, it can be used for wearable aprons or garments which require a flexible, tough, commercial epoxy formulation such as epiclone-4816 as the epoxy matrix. By the way, special epoxy formulations with Gd particles can be used as coated fabrics for, good wear resistance, good hydrolytic resistance, and good ultraviolet light resistance and X-ray attenuation in the textiles industry [230].

REFERENCES

- [1] J. Ramsden, *Nanotechnology: an introduction*. Norwich, N.Y: Elsevier Inc., 2011, pp. 1-14.
- [2] W. R. Caseri, "Nanocomposites of polymers and inorganic particles: preparation, structure and properties," *Mater. Sci. Technol.*, vol. 22, no. 7, pp. 807-817, 2006.
- [3] C. Sanchez, P. Belleville, M. Popall, and L. Nicole, "Applications of advanced hybrid organic-inorganic nanomaterials: from laboratory to market," *Chem. Soc. Rev.*, vol. 40, no. 2, pp. 696-753, 2011.
- [4] C. Sanchez, B. Julian, P. Belleville, and M. Popall, "Applications of hybrid organic-inorganic nanocomposites," *J. Mater. Chem.*, vol. 15, no. 35-36, pp. 3559-3592, 2005.
- [5] A. A. Azeez, K. Y. Rhee, S. J. Park, and D. Hui, "Epoxy clay nanocomposites—processing, properties and applications: a review," *Compos., Part B*, vol. 45, no. 1, pp. 308-320, 2013.
- [6] L. Merad, B. Benyoucef, M. Abadie, and J. Charles, "Characterization and mechanical properties of epoxy resin reinforced with TiO₂ nanoparticles," *Exp. Techniques*, vol. 38, no. 1, pp. 59-66, Jan 2014.
- [7] J. Ma *et al.*, "Fabrication, structure and properties of epoxy/metal nanocomposites," *Macromol. Mater. Eng.*, vol. 296, no. 5, pp. 465-474, 2011.
- [8] S. E. Gwaily, "Galena/(NR+SBR) rubber composites as gamma radiation shields," *Polym Test.*, vol. 21, no. 8, pp. 883-887, 2002.
- [9] M. M. Abdel Aziz and S. E. Gwaily, "Thermal and mechanical properties of styrene-butadiene rubber/lead oxide composites as gamma-radiation shields," *Polym. Degrad. Stab.*, vol. 55, no. 3, pp. 269-274, 1997.
- [10] J. P. McCaffrey, F. Tessier, and H. Shen, "Radiation shielding materials and radiation scatter effects for interventional radiology (IR) physicians," *Med. Phys.*, vol. 39, no. 7, pp. 4537-4546, 2012.
- [11] G. J. Scuderi, G. V. Brusovanik, D. R. Campbell, R. P. Henry, B. Kwon, and A. R. Vaccaro, "Evaluation of non-lead-based protective radiological material in spinal surgery," *Spine J*, vol. 6, no. 5, pp. 577-582, 2006.
- [12] M. Kazempour, M. Saeedimoghadam, F. S. Shooli, and N. Shokrpour, "Assessment of the Radiation Attenuation Properties of Several Lead Free Composites by Monte Carlo Simulation," *J. Biomed. Eng.*, vol. 5, no. 2, p. 67, 2015.

- [13] X. Huang, C. Tan, Z. Yin, and H. Zhang, "25th anniversary article: Hybrid nanostructures based on two-dimensional nanomaterials," *Adv. Mater.*, vol. 26, no. 14, pp. 2185-204, 2014.
- [14] J. F. Fu, L. Y. Shi, Q. D. Zhong, Y. Chen, and L. Y. Chen, "Thermally conductive and electrically insulative nanocomposites based on hyperbranched epoxy and nano-Al₂O₃ particles modified epoxy resin," *Polym. Adv. Technol.*, vol. 22, no. 6, pp. 1032-1041, 2011.
- [15] S. K. Anuar, M. Mariatti, A. Azizan, N. C. Mang, and W. T. Tham, "Effect of different types of silver and epoxy systems on the properties of silver/epoxy conductive adhesives," *J. Mater. Sci. Mater. Electron.*, vol. 22, no. 7, pp. 757-764, Jul 2011.
- [16] C. Poh, M. Mariatti, M. A. Fauzi, C. Ng, C. Chee, and T. Chuah, "Tensile, dielectric, and thermal properties of epoxy composites filled with silica, mica, and calcium carbonate," *J. Mater. Sci. Mater. Electron.*, vol. 25, no. 5, pp. 2111-2119, May 2014.
- [17] A. Yasmin and I. M. Daniel, "Mechanical and thermal properties of graphite platelet/epoxy composites," *Polymer*, vol. 45, no. 24, pp. 8211-8219, Nov 11 2004.
- [18] L. Lei, J. Shan, J. Hu, X. Liu, J. Zhao, and Z. Tong, "Co-curing effect of imidazole grafting graphene oxide synthesized by one-pot method to reinforce epoxy nanocomposites," *Compos. Sci. Technol.*, vol. 128, pp. 161-168, 2016.
- [19] O. Eksik *et al.*, "Nanocomposites of a Cashew Nut Shell Derived Epoxy Resin and Graphene Platelets: From Flexible to Tough," *ACS Sustainable Chem. Eng.*, vol. 4, no. 3, pp. 1715-1721, 2016.
- [20] I. Zaman *et al.*, "Epoxy/graphene platelets nanocomposites with two levels of interface strength," *Polymer*, vol. 52, no. 7, pp. 1603-1611, 2011.
- [21] K. N. Henry Lee, *Handbook of epoxy resins* (McGraw-Hill handbooks). New York: McGraw-Hill, 1967.
- [22] Y. L. Liu, "Flame-retardant epoxy resins from novel phosphorus-containing novolac," *Polymer*, vol. 42, no. 8, pp. 3445-3454, 2001.
- [23] S. Deng, L. Ye, and K. Friedrich, "Fracture behaviours of epoxy nanocomposites with nano-silica at low and elevated temperatures," *J. Mater. Sci.*, vol. 42, no. 8, pp. 2766-2774, 2007.
- [24] C. A. May and Y. Tanaka, (joint author.), C. A. May, Ed. *Epoxy resins: chemistry and technology*, 2 ed. New York: M. Dekker, 1973.
- [25] C. m. S. Pedro Gómez Romero, *Functional hybrid materials*. Weinheim: Wiley-VCH Verlag GmbH & Co., 2004.

- [26] K. R. Long, B. S. Van Gosen, N. K. Foley, and D. Cordier, "The principal rare earth elements deposits of the United States: a summary of domestic deposits and a global perspective," Springer9048186781, 2012.
- [27] C. C. Thompson and Ebrary, *Gadolinium: compounds, production, and applications* (no. Book, Whole). Hauppauge, N.Y: Nova Science Publishers, Inc, 2010.
- [28] S. B. Castor and J. B. Hedrick, "Rare earth elements," *Industrial Minerals volume, 7th edition: Society for Mining, Metallurgy, and Exploration, Littleton, Colorado*, pp. 769-792, 2006.
- [29] N. N. Greenwood and A. Earnshaw, "Chemistry of the Elements (2nd Edition)," Elsevier, 1997.
- [30] K. R. Long, B. S. Van Gosen, N. K. Foley, and D. Cordier, "The principal rare earth elements deposits of the United States: a summary of domestic deposits and a global perspective," in *Non-Renewable Resource Issues*, R. Sinding-Larsen and F.-W. Wellmer, Eds. (International Year of Planet Earth: Springer Netherlands, 2012, pp. 131-155.
- [31] C. C. Thompson and Ebrary, *Gadolinium: compounds, production, and applications* (Chemical Engineering Methods and Technology, no. Book, Whole). Hauppauge, N.Y: Nova Science Publishers, Inc, 2011.
- [32] K. M. Goodenough, F. Wall, and D. Merriman, "The rare earth elements: demand, global resources, and challenges for resourcing future generations," *Nat. Resour. Res.*, pp. 1-16, 2017.
- [33] (2017, 28 August). *Gadolinium*. Available: <https://en.wikipedia.org/wiki/Gadolinium>
- [34] E. May and M. Thoennessen, "Discovery of Samarium, Europium, Gadolinium, and Terbium Isotopes," *At. Data Nucl. Data Tables*, vol. 99, no. 1, 2012.
- [35] A. S. Tremsin, D. F. R. Mildner, W. B. Feller, and R. G. Downing, "Very compact high performance microchannel plate thermal neutron collimators," *IEEE Trans. Nucl. Sci.*, vol. 51, no. 3, pp. 1020-1024, 2004.
- [36] P. Caravan, J. J. Ellison, T. J. McMurry, and R. B. Lauffer, "Gadolinium (III) chelates as MRI contrast agents: structure, dynamics, and applications," *Chem. Rev.*, vol. 99, no. 9, pp. 2293-2352, 1999.
- [37] J. G. Penfield and R. F. Reilly, "What nephrologists need to know about gadolinium," *Nat. Clin. Pract. Nephrol.*, vol. 3, no. 12, pp. 654-668, 2007.

- [38] E. Lewis *et al.*, "Terbium-doped gadolinium oxysulfide ($Gd_2O_2S: Tb$) scintillation-based polymer optical fibre sensor for real time monitoring of radiation dose in oncology," in *Optical Sensing and Detection III*, 2014, vol. 914113: Proc. SPIE 9141.
- [39] B. W. Jeoung, G. Y. Hong, W. T. Yoo, and J. S. Yoo, "Preparation of spherical phosphor (Y, Gd) $BO_3: Eu$ by polymeric-aerosol pyrolysis," *J. Electrochem. Soc.*, vol. 151, no. 10, pp. 213-216, 2004.
- [40] D. S. Kim and R. Y. Lee, "Synthesis and photoluminescence properties of (Y, Gd) $BO_3: Eu$ phosphor prepared by ultrasonic spray," *J. Mater. Sci.*, vol. 35, no. 19, pp. 4777-4782, 2000.
- [41] A. E. Zinnes, B. E. Nevis, and C. D. Brandle, "Automatic diameter control of Czochralski grown crystals," *J. Cryst. Growth*, vol. 19, no. 3, pp. 187-192, 1973.
- [42] P. L. Verplanck, H. E. Taylor, D. K. Nordstrom, and L. B. Barber, "Aqueous stability of gadolinium in surface waters receiving sewage treatment plant effluent, Boulder Creek, Colorado," *Environ. Sci. Technol.*, vol. 39, no. 18, pp. 6923-6929, 2005.
- [43] J. A. Nelson, L. H. Bennett, and M. J. Wagner, "Solution synthesis of gadolinium nanoparticles," *J. Am. Chem. Soc.*, vol. 124, no. 12, pp. 2979-2983, 2002.
- [44] A. C. Faure *et al.*, "Control of the in vivo biodistribution of hybrid nanoparticles with different poly (ethylene glycol) coatings," *Small*, vol. 5, no. 22, pp. 2565-2575, 2009.
- [45] L. E. Van Vlerken and M. M. Amiji, "Multi-functional polymeric nanoparticles for tumour-targeted drug delivery," *Expert Opin. Drug Delivery*, vol. 3, no. 2, pp. 205-16, 2006.
- [46] M. Shokouhimehr *et al.*, "Dual purpose Prussian blue nanoparticles for cellular imaging and drug delivery: a new generation of T 1-weighted MRI contrast and small molecule delivery agents," *J. Mater. Chem.*, vol. 20, no. 25, pp. 5251-5259, 2010.
- [47] R. Lv, S. Gai, Y. Dai, N. Niu, F. He, and P. Yang, "Highly uniform hollow GdF_3 spheres: controllable synthesis, tuned luminescence, and drug-release properties," *ACS Appl. Mater. Inter.*, vol. 5, no. 21, pp. 10806-10818, 2013.
- [48] Q. Ju *et al.*, "Amine-functionalized lanthanide-doped $KGdF_4$ nanocrystals as potential optical/magnetic multimodal bioprobes," *J. Am. Chem. Soc.*, vol. 134, no. 2, pp. 1323-1330, 2011.
- [49] H. K. Cho, H.-J. Cho, S. Lone, D.-D. Kim, J. H. Yeum, and I. W. Cheong, "Preparation and characterization of MRI-active gadolinium nanocomposite particles for neutron capture therapy," *J. Mater. Chem.*, vol. 21, no. 39, pp. 15486-15493, 2011.

- [50] M. W. Ahmad *et al.*, "Potential dual imaging nanoparticle: Gd₂O₃ nanoparticle," *Sci. Rep.*, vol. 5, 2015.
- [51] D. S. Foundation. (2017, 15/08). *Electromagnetic Radiation and Fields*. Available: <http://www.davidsuzuki.org/issues/health/science/enviro-health-policy/electromagnetic-radiation-and-fields/>
- [52] N. Singh, K. J. Singh, K. Singh, and H. Singh, "Comparative study of lead borate and bismuth lead borate glass systems as gamma-radiation shielding materials," *Nucl. Instrum. Methods Phys. Res., Sect. B*, vol. 225, no. 3, pp. 305-309, 2004.
- [53] J. P. McCaffrey, H. Shen, B. Downton, and E. Mainegra-Hing, "Radiation attenuation by lead and nonlead materials used in radiation shielding garments," *Med. Phys.*, vol. 34, no. 2, pp. 530-537, 2007.
- [54] S. Chen, M. Bourham, and A. Rabiei, "Novel light-weight materials for shielding gamma ray," *Radiat. Phys. Chem.*, vol. 96, pp. 27-37, 2014.
- [55] J. P. McCaffrey, E. Mainegra Hing, and H. Shen, "Optimizing non-Pb radiation shielding materials using bilayers," *Med. Phys.*, vol. 36, no. 12, pp. 5586-5594, 2009.
- [56] M. Technologies, "Alpha, beta, gamma, x-ray, and neutron radiation," ed: Mirion Technologies 2017.
- [57] L. Liu, L. He, C. Yang, W. Zhang, R. G. Jin, and L. Q. Zhang, "In situ reaction and radiation protection properties of Gd(AA)₃/NR composites," *Macromol. Rapid Commun.*, vol. 25, no. 12, pp. 1197-1202, 2004.
- [58] S. Nambiar and J. T. Yeow, "Polymer-composite materials for radiation protection," *ACS Appl. Mater. Inter.*, vol. 4, no. 11, pp. 5717-5726, 2012.
- [59] N. Starova, R. Abdrakhmanov, Z. K. Shigapov, and D. Salikhov, "Mechanisms of natural protection of plant ecosystems against radiation," in *Doklady Biological Sciences*, 2002, vol. 385, no. 1, pp. 390-394: Springer.
- [60] C. Yang, L. Liu, Y. Lu, L. He, W. Zhang, and L. Zhang, "Preparation of Tb (Ph_t)₃Phen/rubber composites and characterization of their fluorescent properties," *J. Appl. Polym. Sci.*, vol. 96, no. 1, pp. 20-28, 2005.
- [61] L. Liu *et al.*, "Preparation and luminescence properties of Sm(TTA)₃phen/NBR composites," *Compos. Sci. Technol.*, vol. 67, no. 10, pp. 2199-2207, 2007.
- [62] L. Liu *et al.*, "Novel europium-complex/nitrile- butadiene rubber composites," *Adv. Funct. Mater.*, vol. 15, no. 2, pp. 309-314, 2005.

- [63] S. Ashayer, M. Askari, and H. Afarideh, "Optimal per cent by weight of elements in diagnostic quality radiation shielding materials," *Radiat. Prot. Dosim.*, vol. 149, no. 3, p. 236, 2011.
- [64] M. Kurudirek, M. Büyükyıldız, and Y. Özdemir, "Effective atomic number study of various alloys for total photon interaction in the energy region of 1keV–100GeV," *Nucl. Instrum. Methods Phys. Res., Sect. A*, vol. 613, no. 2, pp. 251-256, 2010.
- [65] S. Mughabghab, "Thermal neutron capture cross sections resonance integrals and g-factors," International Atomic Energy Agency, Vienna440, 2003, vol. 34 issue 12.
- [66] P. Sharma *et al.*, "Gd nanoparticulates: from magnetic resonance imaging to neutron capture therapy," *Adv. Powder Technol.*, vol. 18, no. 6, pp. 663-698, 2007.
- [67] M. Chambers and D. Clarke, "Doped oxides for high-temperature luminescence and lifetime thermometry," *Annu. Rev. Mater. Res.*, vol. 39, pp. 325-359, 2009.
- [68] "Structural Shielding Design for Medical X-Ray Imaging Facilities," in "NCPR Report No. 147 " The National Council on Radiation Protection and Measurements, Bethesda,USA147, 2004.
- [69] L. B. T. La, Y. K. Leong, C. Leatherday, P. I. Au, K. J. Hayward, and L. C. Zhang, "X-ray protection, surface chemistry and rheology of ball-milled submicron Gd₂O₃ aqueous suspension," *Colloids Surf., A*, vol. 501, pp. 75-82, 2016.
- [70] E. G. Christodoulou, M. M. Goodsitt, S. C. Larson, K. L. Darner, J. Satti, and H. P. Chan, "Evaluation of the transmitted exposure through lead equivalent aprons used in a radiology department, including the contribution from backscatter," *Med. Phys.*, vol. 30, no. 6, pp. 1033-1038, 2003.
- [71] E. W. Webster, "Experiments with Medium-Z Materials for Shielding Against Low-Energy X Rays 1," *Radiology*, vol. 86, no. 1, pp. 146-146, 1966.
- [72] E. W. Webster, "Addendum to'Composite materials for x-ray protection'," *Health Phys.*, vol. 61, no. 6, p. 917, 1991.
- [73] P. H. Murphy, Y. Wu, and S. A. Glaze, "Attenuation properties of lead composite aprons," *Radiology*, vol. 186, no. 1, pp. 269-272, 1993.
- [74] H. Ersoy and F. J. Rybicki, "Biochemical safety profiles of Gadolinium-based extracellular contrast agents and nephrogenic systemic fibrosis," *J. Magn. Reson. Imaging*, vol. 26, no. 5, pp. 1190-1197, 2007.
- [75] H. M. Strunk and H. Schild, "Actual clinical use of gadolinium-chelates for non-MRI applications," *Eur. J. Radiol.*, vol. 14, no. 6, pp. 1055-1062, 2004.

- [76] B. C. Ong, Y. K. Leong, and S. B. Chen, "Interparticle forces in spherical monodispersed silica dispersions: Effects of branched polyethylenimine and molecular weight," *J. Colloid Interface Sci.*, vol. 337, no. 1, pp. 24-31, 2009.
- [77] J. Artner *et al.*, "A novel dolo-based diamine as hardener and flame retardant for epoxy resin systems," *Macromol. Mater. Eng.*, vol. 293, no. 6, pp. 503-514, 2008.
- [78] J. P. Foreman, D. Porter, S. Behzadi, K. P. Travis, and F. R. Jones, "Thermodynamic and mechanical properties of amine-cured epoxy resins using group interaction modelling," *J. Mater. Sci.*, vol. 41, no. 20, pp. 6631-6638, 2006.
- [79] P. Bonniau and A. Bunsell, "A comparative study of water absorption theories applied to glass epoxy composites," *J. Compos. Mater.*, vol. 15, no. 3, pp. 272-293, 1981.
- [80] R. J. Jeng, J. R. Wang, J. J. Lin, Y. L. Liu, Y. S. Chiu, and W. C. Su, "Flame retardant epoxy polymers using phosphorus-containing polyalkylene amines as curing agents," *J. Appl. Polym. Sci.*, vol. 82, no. 14, pp. 3526-3538, 2001.
- [81] J. Chen and A. C. Taylor, "Epoxy modified with triblock copolymers: morphology, mechanical properties and fracture mechanisms," *J. Mater. Sci.*, vol. 47, no. 11, pp. 4546-4560, 2012.
- [82] A. Lee and J. D. Lichtenhan, "Thermal and viscoelastic property of epoxy-clay and hybrid inorganic-organic epoxy nanocomposites," *J. Appl. Polym. Sci.*, vol. 73, no. 10, pp. 1993-2001, 1999.
- [83] W. Bascom, R. Cottingham, R. Jones, and P. Peyser, "The fracture of epoxy-and elastomer-modified epoxy polymers in bulk and as adhesives," *J. Appl. Polym. Sci.*, vol. 19, no. 9, pp. 2545-2562, 1975.
- [84] H. C. Kuan, J. B. Dai, and J. Ma, "A reactive polymer for toughening epoxy resin," *J. Appl. Polym. Sci.*, vol. 115, no. 6, pp. 3265-3272, 2010.
- [85] B. S. Patel, *Toughening Mechanisms in Silica-Filled Epoxy Nanocomposites*. Lehigh University, 2016.
- [86] S. S. Vaisakh *et al.*, "Effect of nano-modified SiO₂/Al₂O₃ mixed-matrix micro-composite fillers on thermal, mechanical, and tribological properties of epoxy polymers," *Polym. Adv. Technol.*, vol. 27, no. 7, pp. 905-914, 2016.
- [87] A. Megahed, M. Agwa, and M. Megahed, "Improvement of Hardness and Wear Resistance of Glass Fiber Reinforced Epoxy Composites by the Incorporation of Silica/Carbon Hybrid Nanofillers," *Polym. Plast. Technol. Eng.*, no. just-accepted, 2017.

- [88] M. Suchitra and N. Renukappa, "The Thermal Properties of Glass Fiber Reinforced Epoxy Composites with and without Fillers," in *Macromolecular Symposia*, 2016, vol. 361, no. 1, pp. 117-122: Wiley Online Library.
- [89] H. He, J. Yang, W. Huang, and M. Cheng, "Influence of Nano-Calcium Carbonate Particles on the Moisture Absorption and Mechanical Properties of Epoxy Nanocomposite," *Adv. Polym. Tech.*, 2016.
- [90] G. Miloshevsky, V. Tolkach, G. Shani, and S. Rozin, "Calculated gadolinium atomic electron energy levels and Auger electron emission probability as a function of atomic number Z ," *Nucl. Instrum. Methods Phys. Res., Sect. B*, vol. 192, no. 4, pp. 360-364, 2002.
- [91] K. J. Byeon *et al.*, "Full wafer scale nanoimprint lithography for GaN-based light-emitting diodes," *Thin Solid Films*, vol. 519, no. 7, pp. 2241-2246, 2011.
- [92] W. Gao and Z. Li, "Nano-structured alloy and composite coatings for high temperature applications," *Mat. Res.*, vol. 7, no. 1, pp. 175-182, 2004.
- [93] N. S. Tabrizi, M. Ullmann, V. A. Vons, U. Lafont, and A. Schmidt Ott, "Generation of nanoparticles by spark discharge," *J. Nanopart. Res.*, vol. 11, no. 2, pp. 315-332, 2009.
- [94] R. Ye, J. G. Li, and T. Ishigaki, "Controlled synthesis of alumina nanoparticles using inductively coupled thermal plasma with enhanced quenching," *Thin Solid Films*, vol. 515, no. 9, pp. 4251-4257, 2007.
- [95] Y. Min, M. Akbulut, K. Kristiansen, Y. Golan, and J. Israelachvili, "The role of interparticle and external forces in nanoparticle assembly," *Nat. Mater.*, vol. 7, no. 7, pp. 527-538, 2008.
- [96] R. Vajtai, (editor of compilation.), *Springer handbook of nanomaterials*, 1 ed. Berlin Springer, 2013.
- [97] M. Leparoux, C. Schreuders, J. W. Shin, and S. Siegmann, "Induction Plasma Synthesis of Carbide Nano-Powders," *Adv. Eng. Mater.*, vol. 7, no. 5, pp. 349-353, 2005.
- [98] S. Y. Fu, X. Q. Feng, B. Lauke, and Y. W. Mai, "Effects of particle size, particle/matrix interface adhesion and particle loading on mechanical properties of particulate-polymer composites," *Compos., Part B*, vol. 39, no. 6, pp. 933-961, 2008.
- [99] C. B. Murray, C. Kagan, and M. Bawendi, "Synthesis and characterization of monodisperse nanocrystals and close-packed nanocrystal assemblies," *Annu. Rev. Mater. Sci.*, vol. 30, no. 1, pp. 545-610, 2000.
- [100] Z. Wu *et al.*, "Transparent, Conductive Carbon Nanotube Films," *Science*, vol. 305, no. 5688, pp. 1273-1276, 2004.

- [101] I. Ted Pella. (2014). *Unconjugated gold and silver sols - gold/silver colloids (sols) [Online]*. Available: http://www.tedpella.com/gold_html/goldsols.htm
- [102] G. Polizos, E. Tuncer, I. Sauers, and K. L. More, "Physical properties of epoxy resin/titanium dioxide nanocomposites," *Polym. Eng. Sci.*, vol. 51, no. 1, pp. 87-93, 2011.
- [103] B. Domènech, J. Bastos-Arrieta, A. Alonso, J. Macanás, M. Muñoz, and D. N. Muraviev, "Bifunctional polymer-metal nanocomposite ion exchange materials," in *Ion exchange technologies*: InTech, 2012.
- [104] Q. Guo *et al.*, "Comparison of in situ and ex situ methods for synthesis of two-photon polymerization polymer nanocomposites," *Polymer*, vol. 6, no. 7, pp. 2037-2050, 2014.
- [105] S. Schlabach, R. Ochs, T. Hanemann, and D. V. Szabó, "Nanoparticles in polymer-matrix composites," *Microsyst. Technol.*, vol. 17, no. 2, pp. 183-193, 2011.
- [106] P. P. Edwards and J. M. Thomas, "Gold in a metallic divided state from faraday to present-day nanoscience," *Angew. Chem. Int. Ed.*, vol. 46, no. 29, pp. 5480-5486, 2007.
- [107] V. K. LaMer and R. H. Dinegar, "Theory, production and mechanism of formation of monodispersed hydrosols," *J. Am. Chem. Soc.*, vol. 72, no. 11, pp. 4847-4854, 1950.
- [108] C. B. Murray, S. Sun, W. Gaschler, H. DoyLe, T. A. Betley, and C. R. Kagan, "Colloidal synthesis of nanocrystals and nanocrystal superlattices," *IBM. J. Res. Dev.*, vol. 45, no. 1, pp. 47-56, 2001.
- [109] M. Faraday, "The Bakerian lecture: experimental relations of gold (and other metals) to light," *Philos. Trans. R. Soc. Lond., B, Biol. Sci.*, pp. 145-181, 1857.
- [110] T. Graham, "Liquid diffusion applied to analysis," *J. Chem. Soc.*, vol. 15, pp. 216-270, 1862.
- [111] D. W. Oxtoby, "Nucleation of first-order phase transitions," *Acc. Chem. Res.*, vol. 31, no. 2, pp. 91-97, 1998.
- [112] N. Huige and H. Thijssen, "Production of large crystals by continuous ripening in a stirrer tank," *J. Cryst. Growth.*, vol. 13, pp. 483-487, 1972.
- [113] T. Hoar and J. Schulman, "Transparent water-in-oil dispersions: the oleopathic hydro-micelle," *Nature*, vol. 152, pp. 102-103, 1943.
- [114] M. J. Lawrence and G. D. Rees, "Microemulsion-based media as novel drug delivery systems," *Adv. Drug Deliv. Rev.*, vol. 45, no. 1, pp. 89-121, 2000.
- [115] V. Pillai, P. Kumar, M. Hou, P. Ayyub, and D. Shah, "Preparation of nanoparticles of silver halides, superconductors and magnetic materials using water-in-oil microemulsions as nano-reactors," *Adv. Colloid Interface Sci.*, vol. 55, pp. 241-269, 1995.

- [116] M. A. Malik, M. Y. Wani, and M. A. Hashim, "Microemulsion method: a novel route to synthesize organic and inorganic nanomaterials: 1st nano update," *Arabian J. Chem.*, vol. 5, no. 4, pp. 397-417, 2012.
- [117] M. A. Lopez Quintela, "Synthesis of nanomaterials in microemulsions: formation mechanisms and growth control," *Curr. Opin. Colloid Interface Sci.*, vol. 8, no. 2, pp. 137-144, 2003.
- [118] M. De, S. Bhattacharya, A. Panda, and S. Moulik, "Physicochemistry of mixed systems of water/AOT (surfactant)/alkanol (cosurfactant)/cycloalkanone (oil): a detailed study of phase behavior, salt effect, and conductance properties," *J. Disper. Sci. Technol.*, vol. 30, no. 3, pp. 277-288, 2009.
- [119] J. D. Holmes, P. A. Bhargava, B. A. Korgel, and K. P. Johnston, "Synthesis of cadmium sulfide Q particles in water-in-CO₂ microemulsions," *Langmuir*, vol. 15, no. 20, pp. 6613-6615, 1999.
- [120] P. A. Winsor, "Hydrotrophy, solubilisation and related emulsification processes," *Trans. Faraday Soc.*, 10.1039/TF9484400376 vol. 44, pp. 376-398, 1948.
- [121] N. I. Ivanova, D. S. Rudelev, B. D. Summ, and A. A. Chalykh, "Synthesis of Barium Sulfate Nanoparticles in Water-in-Oil Microemulsion Systems," *Colloid J.*, vol. 63, no. 6, pp. 714-714, 2001.
- [122] C. Xiangzhong *et al.*, "Synthesis of spherical (Y, Gd) BO₃: Eu³⁺ phosphor using W/O emulsion system," *J. Rare Earths*, vol. 24, no. 6, pp. 719-723, 2006.
- [123] M. O. Oyewumi and R. J. Mumper, "Engineering tumor-targeted gadolinium hexanedione nanoparticles for potential application in neutron capture therapy," *Bioconjugate Chem.*, vol. 13, no. 6, pp. 1328-1335, 2002.
- [124] T. K. Tseng, Y. S. Lin, Y. J. Chen, and H. Chu, "A review of photocatalysts prepared by sol-gel method for VOCs removal," *Int. J. Mol. Sci.*, vol. 11, no. 6, pp. 2336-2361, 2010.
- [125] L. L. Hench and J. K. West, "The sol-gel process," *Chem. Rev.*, vol. 90, no. 1, pp. 33-72, 1990.
- [126] B. Fegley, E. A. Barringer, and H. K. Bowen, "Synthesis and characterization of monosized doped TiO₂ powders," *J. Am. Ceram. Soc.*, vol. 67, no. 6, pp. 113-116, 1984.
- [127] A. L. Hector, "Materials synthesis using oxide free sol-gel systems," *Chem. Inform.*, vol. 39, no. 7, pp. 1745-1753., 2008.
- [128] X. Chen and S. S. Mao, "Titanium dioxide nanomaterials: synthesis, properties, modifications, and applications," *Chem. Rev.*, vol. 107, no. 7, pp. 2891-2959, 2007.

- [129] T. Sugimoto, K. Okada, and H. Itoh, "Synthesis of uniform spindle-type titania particles by the gel–sol method," *J. Colloid Interface Sc.*, vol. 193, no. 1, pp. 140-143, 1997.
- [130] A. Chemseddine and T. Moritz, "Nanostructuring titania: Control over nanocrystal structure, size, shape, and organization," *Eur. J. Inorg. Chem.*, vol. 1999, no. 2, pp. 235-245, 1999.
- [131] F. Evanics, P. Diamente, F. C. J. M. Van Veggel, G. J. Stanisz, and R. Prosser, "Water-soluble GdF₃ and GdF₃/LaF₃ nanoparticles physical characterization and NMR relaxation properties," *Chem. Mater.*, vol. 18, no. 10, pp. 2499-2505, 2006.
- [132] M. Pang, X. Liu, and J. Lin, "Luminescence properties of R₂MoO₆: Eu³⁺ (R= Gd, Y, La) phosphors prepared by Pechini sol-gel process," *J. Mater. Res.*, vol. 20, no. 10, pp. 2676-2681, 2005.
- [133] C. Guo, X. Ding, and Y. Xu, "Luminescent properties of Eu³⁺ doped BaLn₂ZnO₅ (Ln= La, Gd, and Y) phosphors by the sol–gel method," *J. Am. Ceram. Soc.*, vol. 93, no. 6, pp. 1708-1713, 2010.
- [134] M. Galceran, M. Pujol, M. Aguiló, and F. Díaz, "Sol-gel modified Pechini method for obtaining nanocrystalline KRE (WO₄)₂ (RE= Gd and Yb)," *Sol-Gel Sci. Technol*, vol. 42, no. 1, pp. 79-88, 2007.
- [135] P. Qiu, N. Zhou, H. Chen, C. Zhang, G. Gao, and D. Cui, "Recent advances in lanthanide-doped upconversion nanomaterials: synthesis, nanostructures and surface modification," *Nanoscale*, vol. 5, no. 23, pp. 11512-11525, 2013.
- [136] S. Rodriguez-Liviano, N. O. Nuñez, S. Rivera Fernández, J. M. De la Fuente, and M. Ocaña, "Ionic liquid mediated synthesis and surface modification of multifunctional mesoporous Eu: GdF₃ nanoparticles for biomedical applications," *Langmuir*, vol. 29, no. 10, pp. 3411-3418, 2013.
- [137] K. M. Lin, C. C. Lin, C. Y. Hsiao, and Y. Y. Li, "Synthesis of Gd₂Ti₂O₇:Eu³⁺, V⁴⁺ phosphors by sol–gel process and its luminescent properties," *J. Lumin.*, vol. 127, no. 2, pp. 561-567, Dec 2007.
- [138] H. Dislich, "Sol-gel: science, processes and products," *J. Non-Cryst. Solids.*, vol. 80, no. 1, pp. 115-121, 1986.
- [139] R. Bazzi *et al.*, "Synthesis and luminescent properties of sub-5-nm lanthanide oxides nanoparticles," *J. Lumin.*, vol. 102, pp. 445-450, 2003.
- [140] J. L. Bridot *et al.*, "Hybrid gadolinium oxide nanoparticles: multimodal contrast agents for in vivo imaging," *J. Am. Chem. Soc.*, vol. 129, no. 16, pp. 5076-5084, 2007.

- [141] L. Faucher, M. I. Tremblay, J. Lagueux, Y. Gossuin, and M. A. Fortin, "Rapid synthesis of PEGylated ultrasmall gadolinium oxide nanoparticles for cell labeling and tracking with MRI," *ACS Appl. Mater. Inter.*, vol. 4, no. 9, pp. 4506-4515, 2012.
- [142] F. Chen *et al.*, "Terbium-doped gadolinium oxide nanoparticles prepared by laser ablation in liquid for use as a fluorescence and magnetic resonance imaging dual-modal contrast agent," *Phys. Chem.*, vol. 17, no. 2, pp. 1189-1196, 2015.
- [143] A. Mignot *et al.*, "A top-down synthesis route to ultrasmall multifunctional Gd-based silica nanoparticles for yheranostic applications," *Chem. Eur. J.*, vol. 19, no. 19, pp. 6122-6136, 2013.
- [144] A. Betke and G. Kickelbick, "Bottom-up, wet chemical technique for the continuous synthesis of inorganic nanoparticles," *Inorganics*, vol. 2, no. 1, pp. 1-15, 2014.
- [145] D. Hari Prasad *et al.*, "Superior sinterability of nano-crystalline gadolinium doped ceria powders synthesized by co-precipitation method," *J. Alloys Compd.*, vol. 495, no. 1, pp. 238-241, 2010.
- [146] I. Muneer, M. A. Farrukh, S. Javaid, M. Shahid, and M. Khaleeq-ur-Rahman, "Synthesis of Gd₂O₃/Sm₂O₃ nanocomposite via sonication and hydrothermal methods and its optical properties," *Superlattices Microstruct.*, vol. 77, pp. 256-266, 2015.
- [147] N. Zhang *et al.*, "Lanthanide hydroxide nanorods and their thermal decomposition to lanthanide oxide nanorods," *Mater. Chem. Phys.*, vol. 114, no. 1, pp. 160-167, 2009.
- [148] L. C. Zhang, Z. Q. Shen, and J. Xu, "Mechanically milling-induced amorphization in Sn-containing Ti-based multicomponent alloy systems," *Mater. Sci. Eng. A*, vol. 394, no. 1, pp. 204-209, 2005.
- [149] P. Yu, L. C. Zhang, W. Zhang, J. Das, K. Kim, and J. Eckert, "Interfacial reaction during the fabrication of Ni₆₀Nb₄₀ metallic glass particles-reinforced Al based MMCs," *Mater. Sci. Eng. A*, vol. 444, no. 1, pp. 206-213, 2007.
- [150] L. C. Zhang, K. Kim, P. Yu, W. Zhang, U. Kunz, and J. Eckert, "Amorphization in mechanically alloyed (Ti, Zr, Nb)-(Cu, Ni)-Al equiatomic alloys," *J. Alloys Compd.*, vol. 428, no. 1, pp. 157-163, 2007.
- [151] H. B. Lu, C. K. Poh, L. C. Zhang, Z. P. Guo, X. B. Yu, and H. K. Liu, "Dehydrogenation characteristics of Ti-and Ni/Ti-catalyzed Mg hydrides," *J. Alloys Compd.*, vol. 481, no. 1, pp. 152-155, 2009.

- [152] L. C. Zhang and H. Attar, "Selective laser melting of Titanium alloys and Titanium matrix composites for biomedical applications: a review," *Adv. Eng. Mater.*, vol. 18, no. 4, pp. 463-475, 2016.
- [153] K. Kendall, "The impossibility of comminuting small particles by compression," *Nature* vol. 272, no. 5655 pp. 710-711, 1978.
- [154] J. T. Hagan, "Impossibility of fragmenting small particles: brittle-ductile transition," *J. Mater. Sci.*, vol. 16, no. 10, pp. 2909-2911, 1981.
- [155] J. E. Field, M. Farhat, and S. M. Walley, "Comminution limit (CL) of particles and possible implications for pumped storage reservoirs," *J. Mater. Sci.*, vol. 49, no. 10, pp. 3780-3784, 2014.
- [156] M. Ullah, M. E. Ali, and S. B. A. Hamid, "Surfactant-assisted ball milling: A novel route to novel materials with controlled nanostructure-a review," *Rev. Adv. Mater. Sci.*, vol. 37, no. 1-2, pp. 1-14, 2014.
- [157] V.-I. Merupo, S. Velumani, K. Ordon, N. Errien, J. Szade, and A.-H. Kassiba, "Structural and optical characterization of ball-milled copper-doped bismuth vanadium oxide (BiVO₄)," *Cryst. Eng. Comm.*, vol. 17, no. 17, pp. 3366-3375, 2015.
- [158] T. Tsuzuki, E. Pirault, and P. McCormick, "Mechanochemical synthesis of gadolinium oxide nanoparticles," *Nanostruct. Mater.*, vol. 11, no. 1, pp. 125-131, 1999.
- [159] T. Tsuzuki, W. T. Harrison, and P. G. McCormick, "Synthesis of ultrafine gadolinium oxide powder by mechanochemical processing," *J. Alloys Compd.*, vol. 281, no. 2, pp. 146-151, 1998.
- [160] M. O. Rasmussen, O. Axelsson, and D. Tanner, "A practical procedure for the solid-phase synthesis of racemic 2,2'-dihydroxy-1,1'-binaphthyl," *Synth. Commun.*, vol. 27, no. 23, pp. 4027-4030, 1997.
- [161] S. F. Nielsen, D. Peters, and O. Axelsson, "The Suzuki reaction under solvent-free conditions," *Synth. Commun.*, vol. 30, no. 19, pp. 3501-3509, 2000.
- [162] Y. Wang, Y. Li, C. Rong, and J. P. Liu, "Sm-Co hard magnetic nanoparticles prepared by surfactant-assisted ball milling," *Nanotechnology*, vol. 18, no. 46, pp. 465701-465704, 2007.
- [163] M. Yue, J. Zhang, H. Zeng, and K. Wang, "Preparation, microstructure, and magnetic properties of bulk nanocrystalline Gd metal," *Appl. Phys. Lett.*, vol. 89, no. 23, pp. 2325041-2325043, 2006.

- [164] Z. Z. Fang, X. Wang, T. Ryu, K. S. Hwang, and H. Sohn, "Synthesis, sintering, and mechanical properties of nanocrystalline cemented tungsten carbide—a review," *Int. J. Refract. Met. Hard Mater.*, vol. 27, no. 2, pp. 288-299, 2009.
- [165] D. Yang *et al.*, "Controllable dielectric performance of polymer composites via the Coulomb-blockade effect with core-shell structured nano-particles," *J. Mater. Chem. C*, vol. 5, no. 31, pp. 7759-7767, 2017.
- [166] C. Li and J. Lin, "Rare earth fluoride nano-/microcrystals: synthesis, surface modification and application," *J. Mater. Chem.*, vol. 20, no. 33, pp. 6831-6847, 2010.
- [167] J. Shan and Y. Ju, "Controlled synthesis of lanthanide-doped NaYF₄ upconversion nanocrystals via ligand induced crystal phase transition and silica coating," *Appl. Phys. Lett.*, vol. 91, no. 12, p. 123103, 2007.
- [168] R. A. Goyer, "Lead toxicity: current concerns," *Environ. Health Perspect.*, vol. 100, p. 177, 1993.
- [169] J. Ma, M. S. Mo, X. S. Du, P. Rosso, K. Friedrich, and H. C. Kuan, "Effect of inorganic nanoparticles on mechanical property, fracture toughness and toughening mechanism of two epoxy systems," *Polymer*, vol. 49, no. 16, pp. 3510-3523, 2008.
- [170] H. Wang *et al.*, "Preparation and radiation shielding properties of Gd₂O₃/PEEK composites," *Polym. Compos.*, vol. 36, no. 4, pp. 651-659, 2015.
- [171] Z. Khakpour, A. Youzbashi, A. Maghsoudipour, and K. Ahmadi, "Synthesis of nanosized gadolinium doped ceria solid solution by high energy ball milling," *Powder Technol.*, vol. 214, no. 1, pp. 117-121, 2011.
- [172] Y. K. Leong and B. C. Ong, "Critical zeta potential and the Hamaker constant of oxides in water," *Powder Technol.*, vol. 134, no. 3, pp. 249-254, 2003.
- [173] P. I. Au, S. Hassan, J. Liu, and Y. K. Leong, "Behaviour of laponite gels: Rheology, ageing, pH effect and phase state in the presence of dispersant," *Chem. Eng. Res. Des.*, vol. 101, pp. 65-73, 2015.
- [174] Y. K. Leong *et al.*, "Controlling attractive interparticle forces via small anionic and cationic additives in kaolin clay slurries," *Chem. Eng. Res. Des.*, vol. 90, no. 5, pp. 658-666, 2012.
- [175] P. J. Scales, S. B. Johnson, T. W. Healy, and P. C. Kapur, "Shear yield stress of partially flocculated colloidal suspensions," *AIChE J.*, vol. 44, no. 3, pp. 538-544, 1998.
- [176] Y. D. Liu and H. J. Choi, "Electrorheological fluids: smart soft matter and characteristics," *Soft. Matter.*, vol. 8, no. 48, pp. 11961-11978, 2012.

- [177] B. J. Park, F. F. Fang, and H. J. Choi, "Magnetorheology: materials and application," *Soft. Matter.*, vol. 6, no. 21, pp. 5246-5253, 2010.
- [178] A. I. Gómez-Merino, F. J. Rubio-Hernández, J. F. Velázquez-Navarro, F. J. Galindo-Rosales, and P. Fortes-Quesada, "The Hamaker constant of anatase aqueous suspensions," *J. Colloid Interface Sci.*, vol. 316, no. 2, pp. 451-456, 2007.
- [179] Y. K. Leong, P. J. Scales, T. W. Healy, D. V. Boger, and R. Buscall, "Rheological evidence of adsorbate-mediated short-range steric forces in concentrated dispersions," *J. Chem. Soc., Faraday Trans.*, 10.1039/FT9938902473 vol. 89, no. 14, pp. 2473-2478, 1993.
- [180] M. Pavlovic, R. Huber, M. Adok-Sipiczki, C. Nardin, and I. Szilagy, "Ion specific effects on the stability of layered double hydroxide colloids," *Soft. Matter.*, vol. 12, pp. 4024-4033, 2016.
- [181] P. M. Dove and C. M. Craven, "Surface charge density on silica in alkali and alkaline earth chloride electrolyte solutions," *Geochim. Cosmochim. Acta*, vol. 69, no. 21, pp. 4963-4970, 2005.
- [182] Y. K. Leong, "Yield stress and zeta potential of nanoparticulate silica dispersions under the influence of adsorbed hydrolysis products of metal ions—Cu (II), Al (III) and Th (IV)," *J. Colloid Interface Sci.*, vol. 292, no. 2, pp. 557-566, 2005.
- [183] Y. K. Leong, P. J. Scales, T. W. Healy, and D. V. Boger, "Effect of particle size on colloidal zirconia rheology at the isoelectric point," *J. Am. Ceram. Soc.*, vol. 78, no. 8, pp. 2209-2212, 1995.
- [184] E. Horváth, I. Szilágyi, L. Forró, and A. Magrez, "Probing titanate nanowire surface acidity through methylene blue adsorption in colloidal suspension and on thin films," *J. Colloid Interface Sci.*, vol. 416, pp. 190-197, 2014.
- [185] Y. K. Leong, D. V. Boger, P. J. Scales, and T. W. Healy, "Interparticle forces arising from adsorbed surfactants in colloidal suspensions: An additional attractive force," *J. Colloid Interface Sci.*, vol. 181, no. 2, pp. 605-612, 1996.
- [186] H. C. Hamaker, "The London-van der Waals attraction between spherical particles," *Physica* vol. 4, no. 10, pp. 1058-1072, 1937.
- [187] E. J. Teh, Y. K. Leong, Y. Liu, B. C. Ong, C. C. Berndt, and S. B. Chen, "Yield stress and zeta potential of washed and highly spherical oxide dispersions—critical zeta potential and Hamaker constant," *Powder Technol.*, vol. 198, no. 1, pp. 114-119, 2010.

- [188] P. I. Au, S. Y. Siow, L. Avadiar, E. M. Lee, and Y. K. Leong, "Muscovite mica and koalin slurries: Yield stress–volume fraction and deflocculation point zeta potential comparison," *Powder Technol.*, vol. 262, pp. 124-130, 2014.
- [189] S. C. Klevenhagen, "Experimentally determined backscatter factors for x-rays generated at voltages between 16 and 140 kV," *Phys. Med. Biol.*, vol. 34, no. 12, p. 1871, 1989.
- [190] E. P. Bertin, *Principles and practice of X-ray spectrometric analysis*, 1st ed. Boston, MA: Springer US, 1975.
- [191] B. Ballsieper, "Laminated lead-free X-ray protection material," US Patent 7 897 949, 2011.
- [192] H. Al-Khaiat and M. Haque, "Effect of initial curing on early strength and physical properties of a lightweight concrete," *Cement concrete res.*, vol. 28, no. 6, pp. 859-866, 1998.
- [193] A. A. Torres-Acosta and A. A. Sagues, "Concrete cracking by localized steel corrosion-geometric effects," *ACI Mater. J.*, vol. 101, no. 6, pp. 501-507, 2004.
- [194] J. Sehgal and S. Ito, "Brittleness of glass," *J. Non-Cryst. Solids*, vol. 253, no. 1, pp. 126-132, 1999.
- [195] J. Chave, H. C. Muller-Landau, T. R. Baker, T. A. Easdale, H. t. Steege, and C. O. Webb, "Regional and phylogenetic variation of wood density across 2456 neotropical tree species," *Ecol. Appl.*, vol. 16, no. 6, pp. 2356-2367, 2006.
- [196] Y. K. Leong, D. V. Boger, P. J. Scales, T. W. Healy, and R. Buscall, "Control of the rheology of concentrated aqueous colloidal systems by steric and hydrophobic forces," *J. Chem. Soc., Chem. Commun.*, vol. 134, no. 7, pp. 639-641, 1993.
- [197] S. Majeed and S. Shivashankar, "Rapid, microwave-assisted synthesis of Gd₂O₃ and Eu: Gd₂O₃ nanocrystals: characterization, magnetic, optical and biological studies," *J. Mater. Chem. A*, vol. 2, no. 34, pp. 5585-5593, 2014.
- [198] G. Liu, G. Hong, J. Wang, and X. Dong, "Hydrothermal synthesis of spherical and hollow Gd₂O₃: Eu³⁺ phosphors," *J. Alloys Compd.*, vol. 432, no. 1, pp. 200-204, 2007.
- [199] H. Zhang and J. F. Banfield, "Interatomic Coulombic interactions as the driving force for oriented attachment," *Cryst. Eng. Comm.*, vol. 16, no. 8, pp. 1568-1578, 2014.
- [200] J. Perrin, *Brownian movement and molecular reality*. London: Taylor & Francis, 1910.
- [201] W. Yu and H. Xie, "A review on nanofluids: preparation, stability mechanisms, and applications," *J. Nanomater.*, vol. 2012, p. 435873, 2012.

- [202] F. Gambinossi, S. E. Mylon, and J. K. Ferri, "Aggregation kinetics and colloidal stability of functionalized nanoparticles," *Adv. Colloid Interface Sci.*, vol. 222, pp. 332-349, 2015.
- [203] Y. K. Leong and B. C. Ong, "Polyelectrolyte-mediated interparticle forces in aqueous suspensions: Molecular structure and surface forces relationship," *Chem. Eng. Res. Des.*, vol. 101, pp. 44-55, 2015.
- [204] J. N. Israelachvili, *Intermolecular and surface forces: revised third edition*. Academic press, 2011.
- [205] A. Faghihnejad and H. Zeng, "Hydrophobic interactions between polymer surfaces: using polystyrene as a model system," *Soft. Matter.*, vol. 8, no. 9, pp. 2746-2759, 2012.
- [206] G. V. Franks, "Zeta potentials and yield stresses of silica suspensions in concentrated monovalent electrolytes: isoelectric point shift and additional attraction," *J. Colloid Interface Sci.*, vol. 249, no. 1, pp. 44-51, 2002.
- [207] S. H. Song, P. Koelsch, T. Weidner, M. S. Wagner, and D. G. Castner, "Sodium dodecyl sulfate adsorption onto positively charged surfaces: monolayer formation with opposing headgroup orientations," *Langmuir*, vol. 29, no. 41, pp. 12710-12719, 2013.
- [208] L. B. T. La, Y. K. Leong, H. P. Watts, P. I. Au, K. J. Hayward, and L. C. Zhang, "A novel approach for the preparation of nanosized Gd₂O₃ structure: the influence of surface force on the morphology of ball milled particles," *Colloids Surf., A*, vol. 506, pp. 13-19, 2016.
- [209] Z. Jia, J. Miao, H.-B. Lu, D. Habibi, W. Zhang, and L. Zhang, "Photocatalytic degradation and absorption kinetics of cibacron brilliant yellow 3G-P by nanosized ZnO catalyst under simulated solar light," *J. Taiwan Inst. Chem. Eng.*, vol. 60, pp. 267-274, 2016.
- [210] J. Miao, Z. Jia, H.-B. Lu, D. Habibi, and L.-C. Zhang, "Heterogeneous photocatalytic degradation of mordant black 11 with ZnO nanoparticles under UV-Vis light," *J. Taiwan Inst. Chem. Eng.*, vol. 45, no. 4, pp. 1636-1641, 2014.
- [211] D. Lin-Vien, N. B. Colthup, W. G. Fateley, and J. G. Grasselli, *The handbook of infrared and Raman characteristic frequencies of organic molecules*. Elsevier, 1991.
- [212] E. D. Risberg, L. Eriksson, J. Mink, L. G. M. Pettersson, M. Y. Skripkin, and M. Sandström, "Sulfur X-ray absorption and vibrational spectroscopic study of sulfur dioxide, sulfite, and sulfonate solutions and of the substituted sulfonate ions X₃CSO₃⁻ (X = H, Cl, F)," *Inorg. Chem.*, vol. 46, no. 20, p. 8332, 2007.

- [213] R. L. Frost, R. Scholz, and A. López, "Raman and infrared spectroscopic characterization of the arsenate-bearing mineral tangdanite— and in comparison with the discredited mineral clinotyrolite," *J. Raman Spectrosc.*, vol. 46, no. 10, pp. 920-926, 2015.
- [214] K. M. K. Reddy, S. Santhisudha, G. Mohan, K. Peddanna, C. A. Rao, and C. Suresh Reddy, "Nano Gd_2O_3 catalyzed synthesis and anti-oxidant activity of new α -aminophosphonates," *Phosphorus Sulfur Silicon Relat. Elem.*, vol. 191, no. 6, pp. 933-938, 2016.
- [215] J. Liu *et al.*, "Sub-10 nm monoclinic Gd_2O_3 : Eu^{3+} nanoparticles as dual-modal nanoprobes for magnetic resonance and fluorescence imaging," *Langmuir*, vol. 30, no. 43, pp. 13005-13013, 2014.
- [216] R. Chen *et al.*, "Parallel comparative studies on mouse toxicity of oxide nanoparticle- and gadolinium-based T1 MRI contrast agents," *ACS nano*, vol. 9, no. 12, pp. 12425-12435, 2015.
- [217] A. Barbosa, L. da Silva, J. Abenojar, M. Figueiredo, and A. Öchsner, "Toughness of a brittle epoxy resin reinforced with micro cork particles: Effect of size, amount and surface treatment," *Compos., Part B*, vol. 114, pp. 299-310, 2017.
- [218] D. Carolan, A. Ivankovic, A. Kinloch, S. Sprenger, and A. Taylor, "Toughened carbon fibre-reinforced polymer composites with nanoparticle-modified epoxy matrices," *J. Mater. Sci.*, vol. 52, no. 3, pp. 1767-1788, 2017.
- [219] Q. Meng, S. Araby, and J. Ma, "Toughening mechanisms in epoxy/graphene platelets," in *Toughening Mechanisms in Composite Materials*, 2015, pp. 73-112.
- [220] F. Hussain, M. Hojjati, M. Okamoto, and R. Gorga, "Review article: polymer-matrix nanocomposites, processing, manufacturing, and application: an overview," *J. Compos. Mater.*, vol. 40, no. 17, pp. 1511-1575, 2006.
- [221] S. Ahmed and F. Jones, "A review of particulate reinforcement theories for polymer composites," *J. Mater. Sci.*, vol. 25, no. 12, pp. 4933-4942, 1990.
- [222] H. Ma, J. Xu, and E. Ma, "Mg-based bulk metallic glass composites with plasticity and high strength," *Appl. Phys. Lett.*, vol. 83, no. 14, pp. 2793-2795, 2003.
- [223] Y. Liu, X. Li, L. Zhang, and T. Sercombe, "Processing and properties of topologically optimised biomedical Ti–24Nb–4Zr–8Sn scaffolds manufactured by selective laser melting," *Mater. Sci. Eng. A*, vol. 642, pp. 268-278, 2015.

- [224] Y. Liu *et al.*, "Microstructure, defects and mechanical behavior of beta-type titanium porous structures manufactured by electron beam melting and selective laser melting," *Acta Mater.*, vol. 113, pp. 56-67, 2016.
- [225] S. Ehtemam-Haghighi, Y. Liu, G. Cao, and L.-C. Zhang, "Phase transition, microstructural evolution and mechanical properties of Ti-Nb-Fe alloys induced by Fe addition," *Mater. Des.*, vol. 97, pp. 279-286, 2016.
- [226] Q. Zhao and S. Hoa, "Toughening mechanism of epoxy resins with micro/nano particles," *Compos. Sci. Technol.*, vol. 41, no. 2, pp. 201-219, 2007.
- [227] F. H. Gojny, M. H. Wichmann, B. Fiedler, and K. Schulte, "Influence of different carbon nanotubes on the mechanical properties of epoxy matrix composites—a comparative study," *Compos. Sci. Technol.*, vol. 65, no. 15, pp. 2300-2313, 2005.
- [228] L. Boogh, B. Pettersson, and J. A. E. Månson, "Dendritic hyperbranched polymers as tougheners for epoxy resins," *Polymer*, vol. 40, no. 9, pp. 2249-2261, 1999.
- [229] S. Zhao, L. S. Schadler, R. Duncan, H. Hillborg, and T. Auletta, "Mechanisms leading to improved mechanical performance in nanoscale alumina filled epoxy," *Compos. Sci. Technol.*, vol. 68, no. 14, pp. 2965-2975, 2008.
- [230] R. W. Stamper, "Flexible epoxy-coated fabric," 1990.
- [231] J. Johnson *et al.*, "Gd₂O₃/GaN metal-oxide-semiconductor field-effect transistor," *Appl. Phys. Lett.*, vol. 77, no. 20, pp. 3230-3232, 2000.

APPENDIX A: STANDARD OPERATION PROCEDURE OF ZETA POTENTIAL ANALAYSIS

1. Preparing a slurry with particles concentration normally from 3% to 5%

$$CP\% = \frac{m_{particle}}{m_{H_2O} + m_{particle}}$$

$$V_{vessel} = \frac{m_{particle}}{D_{particle}} + \frac{m_{H_2O}}{D_{H_2O}} \approx 260ml$$

Density of Gadolinium oxide ($D_{particle}$) = 7.401g/ml

Density of water (D_{H_2O}) = 1g/ml


Weight $m_{particle}$ (g) and then add $m_{H_2O} = 260 - \frac{m_{particle}}{D_{particle}}$ (g). This slurry will be sonicated

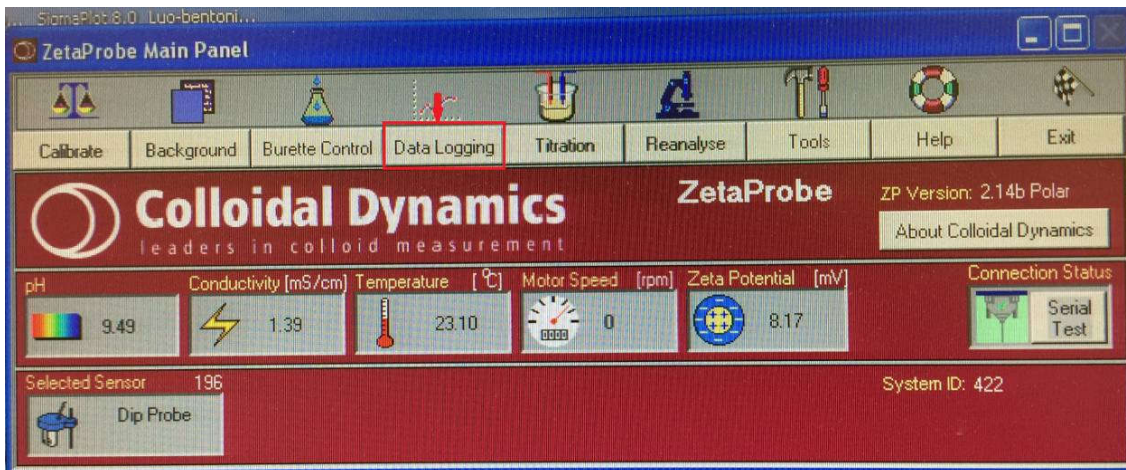
by Branson Digital B30 sonifier, 65-70% amplitude and then transferred into zeta probe clean container

The zeta potential of around 2-5wt% suspensions was measured using Colloidal Dynamic Zeta Probe equipment at different pH condition. The pH of the suspension was changed by an addition of 0.7M KOH or 0.7M HNO₃, via auto-control system.

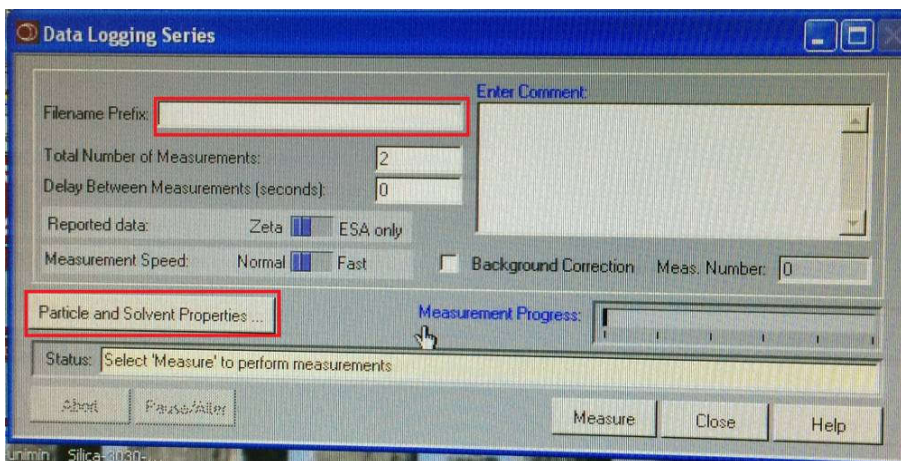
2. Turn on ZetaProbe (Colloidal Dyamic) and calibrate if necessary. Put the slurry into the machine and turn on the stirrer with the speed from 200-250 rpm. Cleaning the pH probe and put it in the slurry and check the value of pH, conductivity ($\mu\text{s}/\text{cm}$).



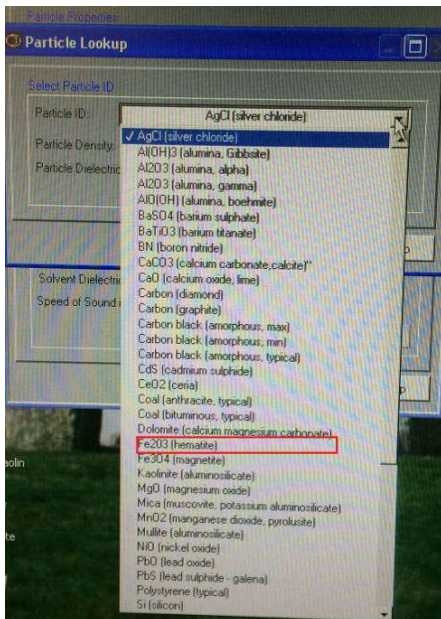
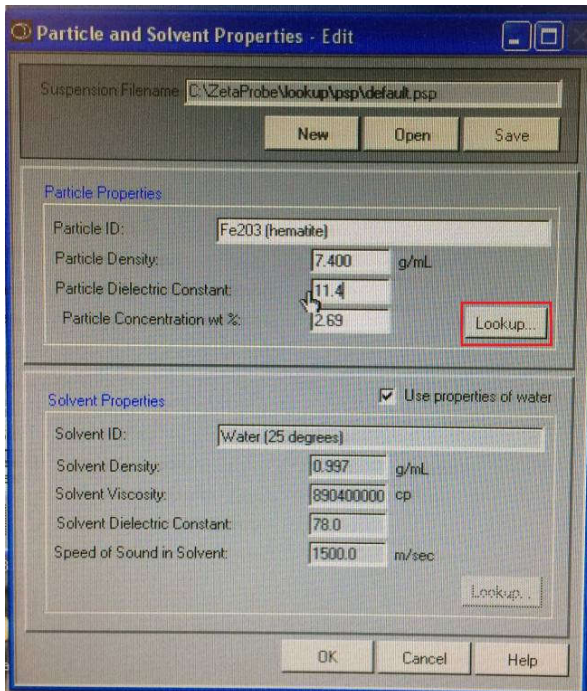
3. Click on the icon  (Zp polar) on computer desktop and then the zeta probe main panel will appear as follow → press on “Data logging”



- On main panel of “Data logging series” , the name of file will be put on “file name prefix” for example “LYLA-Gd-ball milling” → click on “Particle and Solvent Properties”



- On main panel of “Particle and Solvent Properties”, click on “Look up” button of particle properties section. Then the Particle look up panel will be displayed → On “particle ID” choose one of suitable system from the list here we choose Fe_2O_3 → press Ok



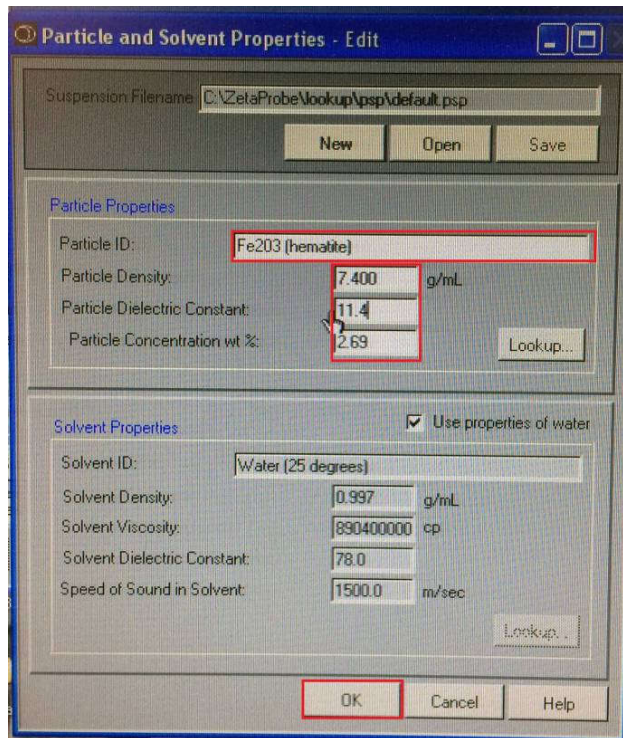
6. After step 5 the panel of “Particle and Solvent Properties” will reappeared → change the value of Particle density, Particles Dielectric Constant , Particle Concentration wt% as follow

Particle density=7.401g/ml

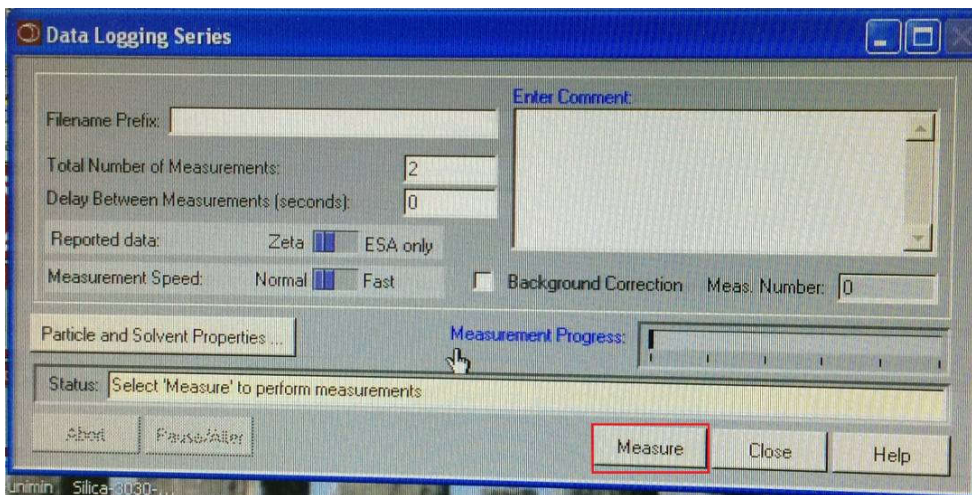
Particles Dielectric Constant= 11.4 [231]

Particle Concentration wt% (from step 1)

→ Press “Ok”



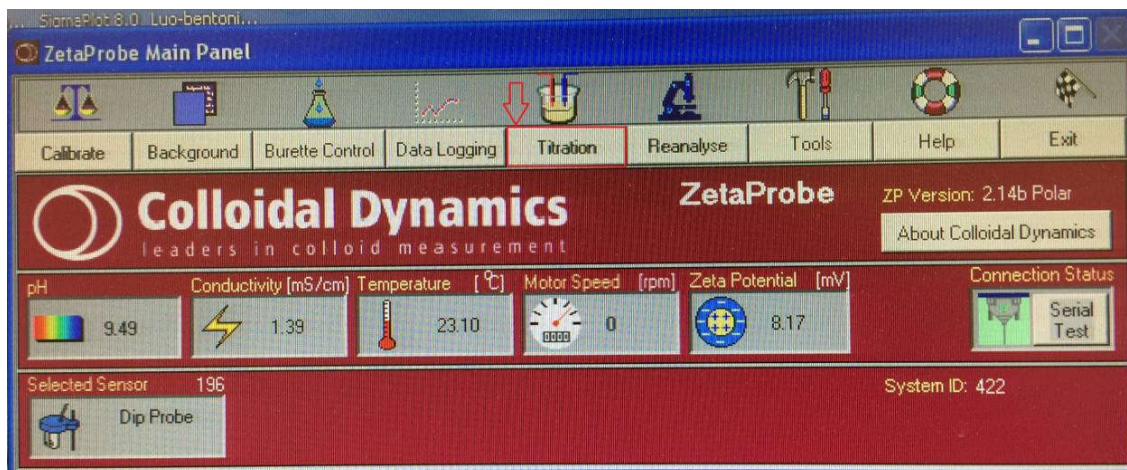
7. Go to “Data logging series” and press measure



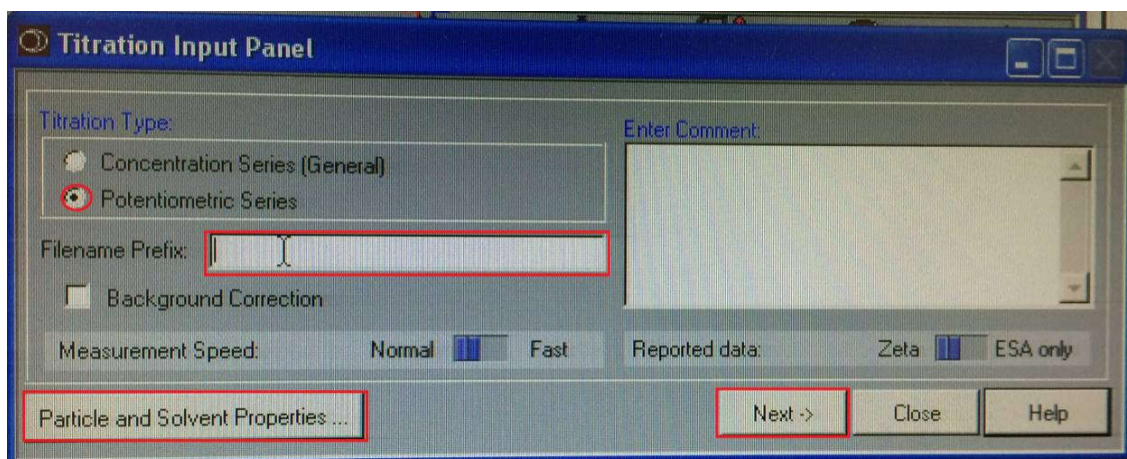
8. After finish the measure stage, the value of pH, Volume and zetapotential will be recorded.
If

- Zeta potential value is >0 → using NaOH or KOH 0.7M to titrate
- Zeta potential value is <0 → using HNO₃ 0.7M to titrate

9. Go back to main panel → click on “Titration”



10. The panel “ Titration Input Panel” appears → click to choose “Potentiometric” → named the samples in “Filename Prefix” → press on “Particle and Solvent Properties” button to check information → click “Next” →



11. Put the pipette probe in slurry to prepare for titration process.
12. On “Potentiometric Series Titration” panel, put the name of titrated solvent in “Acid Id” and “Base Id” and value of Acid and Base concentration. From step 8 put the value of sample volume in the blank.
13. Check the pH value from machine put the “start pH” value in the blank → put the value of “End pH” as you plan → put “pH increment” value on the box (normally 0.5) → press “Titrate”

Potentiometric Series Titration

Auto-Burette Control

Input Titration File:

Background File:

Output File:

Titration Properties

Acid Id: Acid Conc. (left): mole/L

Base Id: Base Conc. (right): mole/L

Sample Volume: mL Equilibration Delay: seconds

Titration

No.	Start pH	End pH	pH Increment	<input type="checkbox"/>
No. 1	<input type="text" value="10.66"/>	<input type="text" value="12.00"/>	<input type="text" value="0.50"/>	<input checked="" type="checkbox"/>
No. 2	<input type="text" value="0.00"/>	<input type="text" value="0.00"/>	<input type="text" value="0.00"/>	<input type="checkbox"/>
No. 3	<input type="text" value="0.00"/>	<input type="text" value="0.00"/>	<input type="text" value="0.00"/>	<input type="checkbox"/>

Titration Results

		Left (Acid)	Right (Base)			
Current pH	<input type="text" value="0.00"/>	<input type="text" value="0.000000"/>	<input type="text" value="0.000000"/>	Current Volume	<input type="text" value="0.000000"/>	
Target pH	<input type="text" value="0.00"/>	Total Volume Added (mL)	<input type="text" value="0.000000"/>	<input type="text" value="0.000000"/>	Vessel Volume	<input type="text" value="300.000000"/>

Show Particle/Solvent Properties

Titration Progress:

Status:

APPENDIX B: X-RAY ATTENUATION EFFICIENCY OF SPECIMENS

Beam energy (kVp)	X-ray attenuation efficiency of 8 mm thickness at different volume fractions							X-ray attenuation efficiency of 16 mm thickness at different volume fractions						
	0	0.004	0.006	0.008	0.01	0.12	0.14	0.004	0.006	0.008	0.01	0.12	0.14	
60	0.18417	0.859	0.9281	0.9455	0.9679	0.9807	0.985	0.9633	0.9867	0.9922	0.9966	0.9984	0.9994	
70	0.18208	0.8467	0.9215	0.9408	0.9634	0.9782	0.983	0.9586	0.9846	0.9913	0.9961	0.9981	0.9993	
80	0.17587	0.8314	0.9125	0.9344	0.9602	0.9759	0.981	0.9544	0.9832	0.9903	0.9959	0.9979	0.9992	
90	0.16569	0.8154	0.9012	0.9267	0.9546	0.9738	0.979	0.9486	0.9807	0.9889	0.9951	0.9977	0.999	
100	0.15932	0.7985	0.8885	0.9148	0.9464	0.9689	0.975	0.9405	0.9765	0.9862	0.9938	0.9968	0.9986	
110	0.15935	0.7793	0.874	0.9023	0.9367	0.9609	0.969	0.9302	0.971	0.9821	0.9915	0.9953	0.9978	
120	0.14892	0.7594	0.857	0.8874	0.9251	0.952	0.961	0.9179	0.9632	0.9767	0.9878	0.9929	0.9964	

Beam energy (kVp)	X-ray attenuation efficiency of 8 mm thickness at different volume fractions							X-ray attenuation efficiency of 16 mm thickness at different volume fractions						
	0	0.004	0.006	0.008	0.01	0.12	0.14	0.004	0.006	0.008	0.01	0.12	0.14	
60	0.18417	0.859	0.9281	0.9455	0.9679	0.9807	0.985	0.9633	0.9867	0.9922	0.9966	0.9984	0.9994	
70	0.18208	0.8467	0.9215	0.9408	0.9634	0.9782	0.983	0.9586	0.9846	0.9913	0.9961	0.9981	0.9993	
80	0.17587	0.8314	0.9125	0.9344	0.9602	0.9759	0.981	0.9544	0.9832	0.9903	0.9959	0.9979	0.9992	
90	0.16569	0.8154	0.9012	0.9267	0.9546	0.9738	0.979	0.9486	0.9807	0.9889	0.9951	0.9977	0.999	
100	0.15932	0.7985	0.8885	0.9148	0.9464	0.9689	0.975	0.9405	0.9765	0.9862	0.9938	0.9968	0.9986	
110	0.15935	0.7793	0.874	0.9023	0.9367	0.9609	0.969	0.9302	0.971	0.9821	0.9915	0.9953	0.9978	
120	0.14892	0.7594	0.857	0.8874	0.9251	0.952	0.961	0.9179	0.9632	0.9767	0.9878	0.9929	0.9964	

APPENDIX C: X-RAY ATTENUATION EFFICIENCY OF Pb SHEETS

Beam energy (kVp)	X-ray attenuation efficiency of pure Pb at different thickness (mm)					
	0.2	0.25	0.3	0.35	0.5	1
60	0.97403	0.986	0.991534	0.995	0.999	1.000
65	0.962434	0.977	0.985859	0.991	0.997	1.000
70	0.948651	0.967	0.978191	0.985	0.995	1.000
75	0.93345	0.955	0.968903	0.978	0.991	0.999
80	0.917615	0.943	0.958525	0.969	0.986	0.999
85	0.901452	0.929	0.947509	0.960	0.981	0.997
90	0.885307	0.916	0.936317	0.951	0.975	0.996
95	0.869092	0.903	0.9252	0.941	0.969	0.994
100	0.853315	0.890	0.91467	0.932	0.963	0.993
105	0.837324	0.877	0.904549	0.924	0.959	0.991
110	0.821643	0.865	0.895048	0.917	0.955	0.991
115	0.806107	0.853	0.885874	0.910	0.951	0.990
120	0.790595	0.841	0.876768	0.903	0.948	0.990

Density of the materials (g/cm ³)					
Gd ₂ O ₃	diionized water	lead	wood	concrete	glass
7.4	1	11.34	0.64	2.4	2.5

Beam energy (kVp)	The thickness of other materials at corresponding radiation attenuation efficiency of 16 mm thick Gd-co
-------------------	---

**APPENDIX D: THE THICKNESS OF LEAD, WOOD, CONCRETE AND GLASS
AT CORRESPONDING RADIATION ATTENUATION EFFICIENCY OF
SPECIMENS**

Beam energy (kVp)	The thickness of other materials at corresponding radiation attenuation efficiency of 10 mm thick Gd ₂ O ₃ aqueous suspension ($\phi_s = 0.082$) (mm)			
	lead	wood	concrete	glass
50	0.152	331.210	18.366	21.615
60	0.173	339.942	19.527	23.752
70	0.229	372.258	20.950	29.377
80	0.295	385.972	27.256	34.247
90	0.354	386.083	31.026	39.478
100	0.400	384.157	33.568	42.168

Beam energy (kVp)	The thickness of other materials at corresponding radiation attenuation efficiency			
	Lead	wood	concrete	glass
60	0.244768161	431.5781028	26.597	32.85962792
70	0.334323351	472.2364689	32.297	41.05153286
80	0.436952022	488.4690572	38.435	48.7826458
90	0.543922594	496.8403772	43.889	79.63331757
100	0.606920232	497.8232862	47.204	59.80422804
110	0.60884292	501.1022332	49.714	61.38584847
120	0.582032153	502.4609727	51.868	61.46955982

	lead	wood	concrete	glass
60	0.395031923	591.1697	40.85817	50.52
70	0.548337063	641.8697	50.99267	63.10
80	0.756265055	681.76	63.47384	77.13
90	0.946322777	691.0285	70.14968	111.5
100	1.060136867	690.2476	73.72233	91.3
110	1.038701865	687.984	76.81694	92.69
120	0.944095537	674.9967	78.97434	91.17

**APPENDIX E: WEIGHT- THICKNESS Gd₂O₃/EPOXY NANOCOMPOSITE
(g/cm²) AT DIFFERENT PARTICLE VOLUME FRACTIONS**

	Volume fraction ϕ_s	0.04	0.06	0.08	0.1	0.12	0.14
8 mm	Weight- thickness Gd ₂ O ₃ (g/cm ²)	0.231	0.346	0.462	0.578	0.693	0.826
	Weight- thicknessEpoxy (g/cm ²)	0.838	0.821	0.804	0.787	0.770	0.750
	Weight- thickness Gd ₂ O ₃ /epoxy composite (g/cm ²)	1.069	1.167	1.265	1.365	1.463	1.577
16 mm	Weight- thickness Gd ₂ O ₃ (g/cm ²)	0.461	0.693	0.923	1.155	1.386	1.652
	Weight- thicknessEpoxy (g/cm ²)	1.676	1.642	1.607	1.574	1.540	1.501
	Weight- thickness Gd ₂ O ₃ /epoxy composite (g/cm ²)	2.137	2.334	2.530	2.729	2.926	3.153